A STEADY STATE THERMAL HYDRAULIC ANALYSIS METHOD FOR PRISMATIC GAS REACTORS

A Thesis
Presented to
The Academic Faculty

By

Alexander J Huning

In Partial Fulfillment
Of the Requirements for the Degree
Masters of Science in Nuclear Engineering

Georgia Institute of Technology

May, 2014

A STEADY STATE THERMAL HYDRAULIC ANALYSIS METHOD FOR PRISMATIC GAS REACTORS

Approved by:

Dr. Srinivas Garimella, Co-Advisor
School of Mechanical Engineering
Georgia Institute of Technology

Dr. Farzad Rahnema, Co-Advisor
School of Mechanical Engineering
Georgia Institute of Technology

Dr. Samuel Graham
School of Mechanical Engineering
Georgia Institute of Technology

Date Approved: December 20th, 2013

ACKNOWLEDGEMENTS

I would like to thank my advisors Dr. Srinivas Garimella and Dr. Farzad Rahnema for giving me this opportunity to pursue graduate school and initiate my career. I am extremely grateful for their guidance and mentoring.

I would also like to thank my fellow students of both the Sustainable Thermal Systems Laboratory and Computational Reactor and Medical Physics Laboratory for their kindness, friendship and help as I progress through my graduate studies. Of these students, I am especially grateful of Alex Rattner and Kevin Connolly whose conversations and review of my work has helped me form ideas and address deficiencies wherever present.

I would also like to thank Dr. Samuel Graham for his participation and guidance.

TABLE OF CONTENTS

Page

CHAPTER

LIST OF TABLES

LIST OF FIGURES

NOMENCLATURE

Symbols

a	unit cell surface area
A	channel pressure drop linear constant
B	channel pressure drop linear slope
c_P	constant pressure specific heat
D_H	channel hydraulic diameter
f	friction factor
g	gravitational acceleration
h	heat transfer coefficient
k	thermal conductivity
l	unit cell conduction length
L	channel length
$\dot{m}$	mass flow rate
n	unit normal
Nu	Nusselt number
P	pressure
Pr	Prandtl number
q	heat flux
q'''	volumetric heat rate
Q	heat transfer rate
R	universal gas constant
Re	Reynolds number
S	surface
t	time

T	temperature
v	velocity
V	volume
z	elevation

Greek Letters

ε	surface roughness
π	pi
ρ	density

Sub-scripts and Super-scripts

(0)	iteration 0
(1)	iteration 1
(2)	iteration 2
ave	average
conv	convection
e	outlet
ent,hy	hydrodynamic entrance length
gen	generation
i	inlet
n	channel number
N	number of channels
s	surface index
tot	total

SUMMARY

A new methodology for the accurate and efficient determination of steady state thermal hydraulic parameters for prismatic high temperature gas reactors is developed. Two conceptual reactor designs under investigation by the nuclear industry include the General Atomics GT-MHR and the Department of Energy MHTGR-350. Both reactors use the same hexagonal prismatic block, TRISO fuel compact, and circular coolant channel array design.

Steady state temperature, pressure, and mass flow distributions are determined for the base reference designs and also for a range of values of the important parameters. Core temperature distributions are obtained with reduced computational cost over more highly detailed computational fluid dynamics codes by using efficient, correlations and first-principles-based approaches for the relevant thermal fluid and thermal transport phenomena. Full core 3-D heat conduction calculations are performed at the individual fuel pin and lattice assembly block levels. The fuel compact is treated as a homogeneous medium with heat generation. A simplified 1-D fluid model is developed to predict convective heat removal rates from solid core nodes. Downstream fluid properties are determined by performing a channel energy balance down the axial node length. Channel exit pressures are then compared and inlet mass flows are adjusted until a uniform outlet pressure is reached. Bypass gaps between assembly blocks as well as coolant channels are modeled. Finite volume discretization of energy, and momentum conservation equations are then formed and explicitly integrated in time. Iterations are performed until all local core temperatures stabilize and global convective heat removal matches heat generation.

Several important observations were made based on the steady state analyses for the MHTGR and GT-MHR. Slight temperature variation in the radial direction was observed for uniform radial powers. Bottom-peaked axial power distributions had slightly higher peak temperatures but lower core average temperatures compared to top and center-peaked power distributions. The same trend appeared for large bypass gap sizes cases compared to smaller gap widths. For all cases, peak temperatures were below expected normal operational limits for TRISO fuels. Bypass gap flow for a 3 mm gap width was predicted to be between 10 and 11% for both reactor designs. Single assembly hydrodynamic and temperature results compared favorably with those available in the literature for similar prismatic HTGR thermal hydraulic, computational fluid dynamics analyses.

The method developed here enables detailed local and core wide thermal analysis with minimal computational effort, enabling advanced coupled analyses of high temperature reactors with thermal feedback. The steady state numerical scheme also offers a potential for select transient scenario modeling and a wide variety of design optimization studies.

1. INTRODUCTION

High Temperature Gas-Cooled Reactor (HTGR) development began in the mid-1960s along with the development of high-temperature particle fuels. The first HTGR prototype reactors included the Dragon reactor (1965) in the UK and Peach Bottom Unit 1 (1966) in the US which were both helium-cooled graphite-moderated reactors. Helium was selected as the gas of choice due to its inert nuclear and chemical properties. Graphite was selected as the moderator of choice due to its neutron moderating capabilities, and for its resilience to high temperatures and low interaction with other materials.

The Fort St. Vrain Generating Station (1976) in Platteville, Colorado laid the foundation for future prismatic HTGR designs. It was shut down after ten years of operation. Variants of the fuel assembly block design used in Fort St. Vrain are employed today in modern prismatic HTGR designs.

1.1 Very High Temperature Reactor (VHTR) Background

HTGRs are gas reactor systems with coolant outlet temperatures up to 850°C. The VHTR is distinct from HTGRs as its coolant outlet temperature ranges from 850°C to 1000°C. Because many conceptual designs assume outlet temperatures close to 850°C, the terms VHTR and HTGR are often used interchangeably. Higher outlet temperatures offer increased cycle efficiency and enable many coupled process heat applications. Achieving higher outlet temperatures requires advanced high temperature materials and fuels such as TRI-ISOtropic (TRISO-coated) fuels. Minimizing reactor internal structural temperatures also becomes a large concern.

The need for the VHTR is driven by goals set forth by the Generation IV International Forum (GIF) (U.S. DOE, 2002). These goals that the VHTR must meet are encapsulated into four focus areas:

1. Sustainable nuclear energy: meets clean air objectives, manages nuclear waste and notably reduces the long-term stewardship burden
2. Economic competitiveness: has a clear life-cycle cost advantage over other energy sources and has a level of financial risk comparable with other energy projects.
3. Safety and reliability: will excel in safety and reliability during normal operation and have a very low likelihood and degree of reactor core damage for all potential accident conditions.
4. Proliferation resistance: increases the assurance that they are a very unattractive and the least desirable route for diversion or theft of weapons-usable materials, and provides increased physical protection against acts of terrorism.

The U.S. commitment to the GIF was solidified by the Next Generation Nuclear Plant (NGNP) project. The VHTR was selected out of six reactor designs because it was deemed to be the nearest-term reactor concept that also has the capability to efficiently produce hydrogen (Ryskamp, 2003). The NGNP was formally established by the Energy Policy Act of 2005 with the purpose of designing, licensing and constructing a demonstration plant of either the pebble bed or prismatic VHTR designs (U.S. DOE, 2010). The first phase of the NGNP was to publish conceptual design reports for both the prismatic and pebble-bed reactor systems. In August of 2010, these design reports were completed for two different pebble-bed and four different prismatic reactor system variations (Gibbs, 2010). The selection of hydrogen production technology, and TRISO fuels research were also key components of Phase I activities. The second phase is to finalize the NGNP design and submit a combined operating and license application (COLA) to the Nuclear Regulatory Commission (NRC). It was ultimately determined by the Nuclear Energy Advisory Committee (NEAC) reporting to Department of Energy (DOE) Secretary Dr. Steven Chu that NGNP is not ready to proceed to Phase II actives due to a number of reasons, chief among which was a lack of a 50/50 cost sharing agreement between the DOE and an industry partner (U.S. DOE, 2011).

Even though no formal cost sharing agreement is in place, a number of companies have shown interest in HTGR technology for various process heat applications besides hydrogen production, and formed the NGNP Industry Alliance. These companies include reactor vendors such as AREVA and Westinghouse, and potential process heat buyers such as Dow, Conoco Phillips, and Entergy. In February of 2012, the NGNP Industry Alliance selected AREVA’s prismatic HTGR reactor design over the other reactor systems identified during Phase I of NGNP (NGNP Industry Alliance, 2012). Other VHTR and HTGR prismatic reactor designs include the General Atomics GT-MHR and the DOE MHTGR.

An advantage of the prismatic VHTR over existing and many other conceptual nuclear reactors is its ability to provide a supply of high temperature heat for cogeneration applications. The initial intent of the NGNP was primarily for hydrogen production using high temperature steam electrolysis (HTSE). In a DOE study (Demick, 2007), HTSE could supply up to 25% of the hydrogen market that is currently driven by steam methane reforming. In addition to hydrogen production, process heat produced by the NGNP could offer an alternative to coal-fired cogeneration plants, or be used to drive coal gasification processes. HTGR driven process heat applications remain a promising option as global energy demand increases and as increasingly strict emission limitations restrict fossil fuel heat sources.

1.2 GT-MHR Reactor Summary

The two HTGR designs investigated in this thesis include the General Atomics Gas Turbine Modular Helium Reactor (GT-MHR) and the Modular High Temperature Gas Reactor (MHTGR). Figures 1.1 and 1.2 are reproduced from the GT-MHR conceptual design report (General Atomics, 1996). Figure 1.3 is reproduced from the MHTGR Draft Pre-application Safety report (Williams et al., 1989).

The GT-MHR is a General Atomics high temperature gas reactor design that was a collaborative effort by several participating organizations including ABB Combustion Engineering, General Atomics, Oak Ridge National Laboratory, Bechtel, and others. Design work was initiated in 1993 and funded by the U.S. Department of Energy. The final design was completed in 1996. The main design work was aided by previous experience with earlier designs such as MHTGR. The design thermal power rating is 600 MW.

The core is composed of prismatic hexagonal graphite blocks arrayed in rings: an inner reflector region, an annular active fuel region, and an outer reflector region. Helium coolant flows downward through the active fuel region, which consists of blocks with cylindrical holes for core heat removal and through any gaps between assembly blocks. Fuel consists of TRISO particles pressed into cylindrical compacts and arrayed in active fuel region blocks. Both the inner and outer reflector blocks are solid graphite. A radial cross section view of the core from the GT-MHT conceptual design report is shown in Figure 1.1.

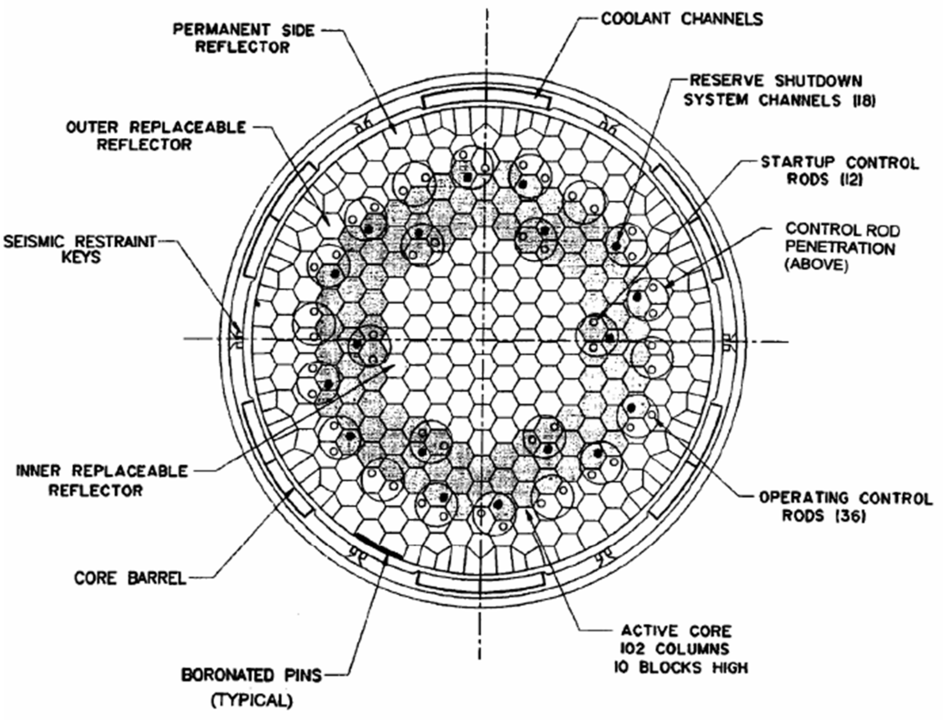

Figure 1.1 GT-MHR core arrangement, General Atomics (1996)

The core is arranged 10 assembly blocks high with an additional reflector block layer above and below the core. There are six types of graphite assembly blocks: solid inner or outer replaceable reflector block, solid permanent side reflector block, reflector block with an operating control rod hole, standard active fuel assembly, fuel assembly block with a reserve shutdown hole, and fuel assembly block with a startup control rod hole. The shutdown system channel is only 95.25 mm in diameter compared to the control rod hole, which is 101.6 mm in diameter.

The reactor is composed of three sections: the lower vessel head and plenum, the core, and the upper vessel head and plenum. An axial cross section view of the vessel from the GT-MHR conceptual design report is show in Figure 1.2.

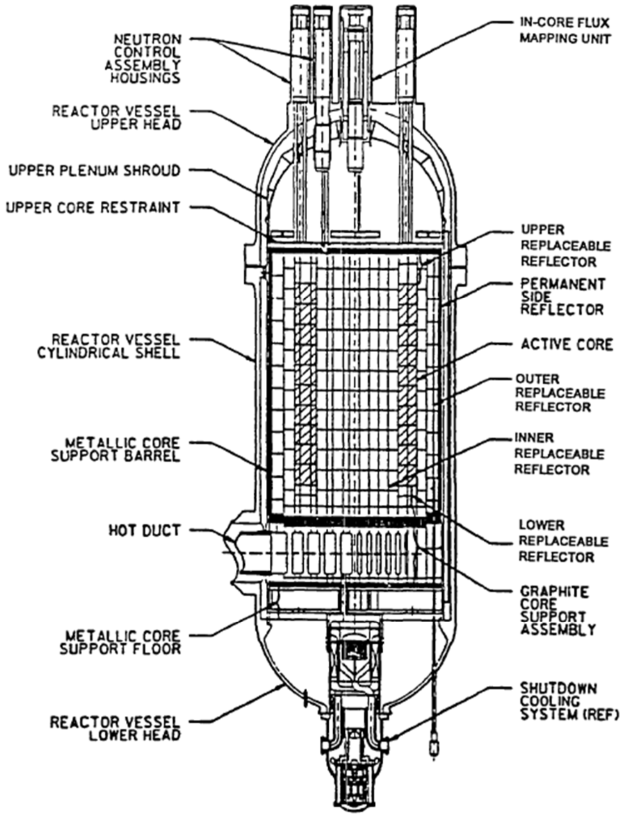

Figure 1.2 GT-MHR reactor vessel elevation view, General Atomics (1996)

The coolant enters the cold duct at the base of the core, travels upward along the sides of the vessel, collects in the upper plenum, flows downward through the core, collects in the lower plenum, and finally travels outward through the hot duct. The cold and hot leg pipes are contained in a single double-walled vessel duct that connects the vessel to the primary conversion unit (PCU). The GT-MHR was originally designed to have a direct Brayton cycle PCU. Later VHTR designs substituted this PCU for an intermediate heat exchanger for process heat applications in addition to power generation.

One negative aspect related to the feasibility of HTGRs is their capital cost, specifically of the reactor vessel. The GT-MHR dimensions are large in comparison to other reactor designs. The active core length is 7.93 m. The total length from the top of the neutron control assembly housings to the base of the shutdown cooling system is 31.2 m. The outer diameter of the cross vessel duct is 2.28 m. The vessel inner diameter is 7.22 m with a wall thickness of 260 mm. These dimensions, when compared to a typical pressurized water reactor, are a factor of ~1.8 times larger in the radial direction, ~2.0 times larger in the axial direction, and ~1.2 times larger in vessel wall thickness. Thermal power is lower by a factor of 4. However, the vessel dimensions are justified when considering the system as a whole. Economic gains over other reactor designs are expected from other areas, in particular the coupled process heat applications.

1.3 MHTGR Reactor Summary

The MHTGR is a U.S. Department of Energy high temperature reactor design that is a predecessor to the GT-MHR. Like the GT-MHR, it was designed with the support of a team consisting of General Atomics, ABB Combustion Engineering, Bechtel, Oak Ridge National Laboratory, and others. Design work started in 1984. The preliminary safety information document for the MHTGR was completed in 1986 with the complete draft pre-application for MHTGR being completed in 1989. The design thermal power rating is 350 MW. The core design of the MHTGR is similar to the GT-MHR. It is also composed of three graphite hexagonal block regions. A core arrangement diagram is shown in Figure 1.3.

The core is arranged 10 assembly blocks high with an upper and lower reflector block layer. These assembly block types are similar to those employed in the GT-MHR with one less assembly block type. In the MHTGR, there are standard fuel assembly blocks and fuel assemblies with reserve shutdown channels, but none with any start up control rod holes as in the GT-MHR.

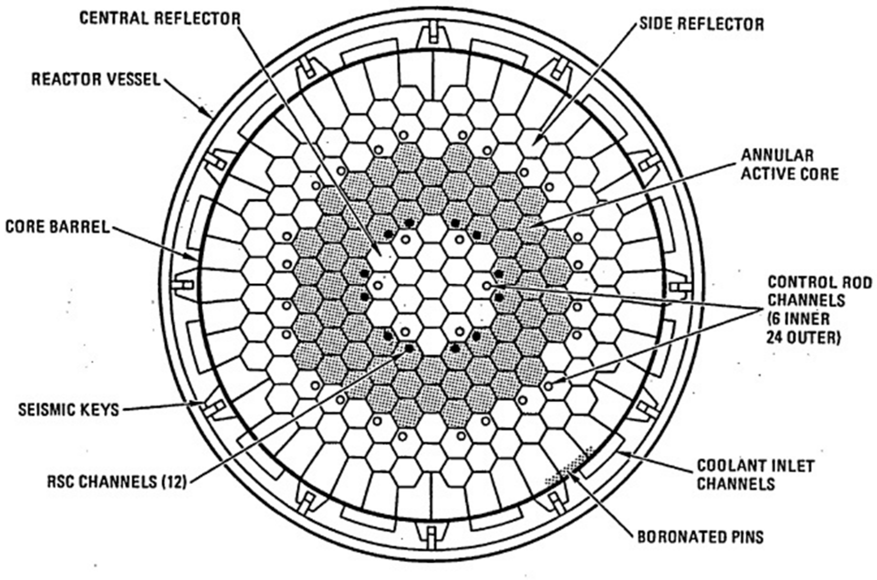

Figure 1.3 MHTGR core arrangement, Williams et al. (1989)

The reactor vessel, internals, and dimensions are exactly the same as the GT-MHR. The intermediate heat exchanger for the MHTGR was designed as a steam generator. The secondary side uses a steam Rankine cycle for power conversion.

Both the MHTGR and GT-MHR utilize the same containment and passive containment heat removal systems. The Reactor Cavity Cooling System (RCCS) is a passive air cooled loop that is connected to a series of ambient air cooled towers. In an accident, the vessel heats up and transfers heat by conduction and radiation to the containment walls. The Reactor Cavity Cooling System (RCCS) then removes heat from the containment walls by natural circulation of ambient air.

1.4 Design Comparisons

Both the GT-MHR and MHTGR use similar assembly and fuel designs. The primary difference between the designs is that the MHTGR has a core thermal power of 350 MW while the GT-MHR is designed for an operating thermal power of 600 MW.

This leads to a smaller core for the MHTGR. Typical thermal design parameters of both reactors are provided in Table 1.1.

Table 1.1 Comparison of Thermal Design Parameters

Parameter	GT-MHR	MHTGR
Core Thermal Power	600 MW	350 MW
Power Density	6.6 MW/m^3	5.9 MW/m^3
Operating Pressure	7.0 MPa	6.4 MPa
Inlet Temperature	490 °C	260 °C
Outlet Temperature	850 °C	690 °C
Core Flow Rate	320 kg/s	157.1 kg/s

The lower thermal power and outlet temperature of the MHTGR allows for a greater margin of safety in the event of an accident such as loss of flow. The next chapter of this thesis will show lower maximum fuel and graphite temperatures for the MHTGR compared to the GT-MHR at steady state.

In addition to the thermal parameters listed in Table 1.1, design parameters common to both the GT-MHR and MHTGR are shown in Table 1.2.

Table 1.2 Design Parameters Common to the GT-MHR and MHTGR

Parameter	Value
Fuel Compact Outer Diameter	12.45 mm
Fuel Gap Outer Diameter	12.70 mm
Fuel Pitch	18.79 mm
Large Coolant Channel Diameter	15.86 mm
Small Coolant Channel Diameter	12.70 mm
Shutdown Hole Diameter	95.25 mm
Control Rod Hole Diameter	0.102 m
Assembly Length	0.793 m
Assembly Diameter	0.360 m
Nominal Assembly Bypass Gap	3.12 mm
Graphite Surface Roughness	10 µm

Fortunately, assembly dimensions between the GT-MHR and MHTGR are identical, and the only geometrical difference between the designs is core assembly arrangement. This leads to an identical discretization and mesh for both designs. No additional material properties are needed for either design beyond graphite, helium, and fuel compact material.

1.5 Scope of Current Research

In the current investigation, a steady state thermal hydraulic method capable of predicting the whole-core, 3-D, temperature, pressure and mass flow distribution is developed. This investigation focuses on the active core region, because that is where the primary safety and normal operation concerns lie. The developed method is then applied to the GT-MHR and the MHTGR to assess its accuracy, computational performance, and gain preliminary insights into the operational design of HTGRs. Boundary conditions, thermal operating parameters, and geometric specifications are taken from safety analysis documents for both designs.

The need for a new method is seen when comparing existing methods and while attempting to address the challenging problems of advanced reactor designs such as the HTGR. As the next chapter will show, existing core thermal hydraulic methods either focus on a small fraction of the total core with a high degree of accuracy, or analyze the whole core by grouping regions, resulting in an efficient but low fidelity calculation. The method presented here attempts to fill an intermediate category of needs by retaining some of the accuracy of a fine mesh solver while running in an efficient enough manner that enables whole-core level calculations.

Whole-core thermal hydraulic analysis methods are needed for HTGRs because of their complex features and the unique advantages that they offer over light and heavy water reactors. The GT-MHR was originally designed only for enriched uranium fuel. Recently, there has been significant interest in using HTGRs for fuel cycle improvement and nuclear waste reduction (Tsvetkov et al, 2006). This is achieved by replacing standard enriched uranium fuel assembly blocks with fuel blocks containing other actinide fuels such as thorium and plutonium. In such cases, the spectrum shifts slightly higher in energy, which allows for the capture of more fast neutrons, and is subsequently more attractive for fuel cycle enhancement. These new assembly block configurations introduce new temperature gradients that are more difficult to model effectively with broad scale or system level methods. New core level configurations make it more difficult for fine scale or single assembly analyses to capture core environment effects.

The method presented here will be able to predict whole-core temperature profiles that capture the temperature gradients within each assembly block and fuel compact. This will allow for design of novel assembly block and core configurations that could enhance the fuel cycle and make HTGRs more attractive.

1.6 Organization of Thesis

The remainder of this thesis is organized as follows:

- Chapter 2 presents and overview of the available literature on core heat transfer and fluid flow modeling of prismatic high temperature gas reactors.
- Chapter 3 presents the methodology for determining core-wide steady-state thermal hydraulic parameters such as temperature, pressure, and mass flow distributions.
- Chapter 4 describes the numerical scheme and implementation of the method.
- Chapter 5 presents a summary of results of the steady-state analysis for both reactor designs.
- Chapter 6 presents conclusions based on the results and suggests areas of further research.

2. LITERATURE REVIEW

The VHTR has received renewed interest due to its ability to provide a clean source of high temperature heat for industrial process applications, in addition to electrical power generation. Modeling and prediction of core thermal hydraulic behavior is essential for both normal operation and transient safety. Thermal hydraulic modeling studies for early gas-cooled reactor designs such as Fort Saint Vrain and Peach Bottom Unit 1 are limited and consist mainly of support calculations for NRC safety analysis reports. Thermal analysis methods for these early HTGRs relied on sets of independent codes that employed simplistic approximations for flow, core, assembly and fuel heat transfer modeling. Table 1 summarizes the set of thermal analysis codes described in detail in a General Atomics report (Shenoy and McEachern, 1974).

Table 2.1 Early HTGR Thermal Analysis Codes (Shenoy and McEachern, 1974)

Code Name	Purpose	Method
FLAC	To determine flow distribution in an arbitrary cross connected flow network; e.g., coolant flow in coolant channel and gaps between blocks in a refueling region.	Solves 1-D momentum equation for incompressible flow, and solves continuity and energy equations. Density changes in gas are modeled.
POKE	To determine, under constraints, steady state orifice valve position, coolant mass flow, coolant temperature, and fuel temperature distribution in HTGR core made up of many parallel coolant channels connecting two plenums.	Steady-state mass and momentum conservation equations for parallel channels, using crossflow correlations, are solved using finite differences for an imposed power distribution. Equivalent conductances from HEXT are used to calculate radial temperature profile within unit cell.

Table 2.1 (continued).

Code Name	Purpose	Method
DEMISE **DEMICE**	To determine steady-state 3-D temperature distribution and flow distribution in 1/2 columns of standard elements (DEMISE) and control elements (DEMICE).	Temperature distribution in network model of 1 /2 column is solved using successive point iteration. Flow distribution is calculated by balancing pressure drop in all coolant passages.
BACH	To calculate steady-state core power/flow ratio to achieve a desired maximum fuel temperature in a specified refueling region of a variable orificed, multiple, parallel channel HTGR core. Kernel migration rate within the fuel is determined.	Coolant channel mass flow is calculated by balancing pressure drop for a single channel. Calculates gas temperatures from energy balance equations. Radial temperature drops in channel are evaluated by calculating local heat flux and appropriate conductances from HEXT model.
HEXT	To determine steady-state temperature distribution and equivalent thermal conductances in fuel, fuel-moderator gap, and moderator in a unit cell of HTGR type fuel elements	Solves heat conduction equation for a particular 2-D geometric configuration.
TREVER	To determine, from given power distribution histories, time histories of steady-state coolant, graphite, and fuel temperatures and temperature gradients for a region. To determine time and space distribution of coating failure.	Solves 1-D (radial) steady-state heat transfer, coolant distributions from POKE, and equivalent conductances from HEXT. Uses experimentally determined correlations to calculate particle coating failure.
TAC-2D	General purpose 2-D steady-state and time dependent thermal analysis of specific core segments.	Solves 2-D heat conduction equation by finite differences using implicit iteration method.

Table 2.1 (continued).

Code Name	Purpose	Method
DETRAC	To determine time histories of coolant, graphite and fuel temperatures within region average and local hot channels during transient operation from given transient power distribution history and given core total power, total flow, helium inlet temperature, and pressure response.	Solves 1-D nodal transient heat transfer equations with no axial conduction or radial conduction between channels. Uses equivalent conductances from HEXT code in calculating fuel and graphite temperatures within a channel. Coolant channel flows calculated by balancing pressure drop across individual channels.

Later reactor designs including the MHTGR and GT-MHR use the same or similar set of codes as those listed above to perform thermal analysis for safety analysis and conceptual design reports. The central modeling technique of these analyses is the equivalent fuel-moderator-coolant triangular unit cell or node. The advantage of this approach is that a single equivalent conductance can be used for each node within the assembly, and a simple homogenous geometry is formed, thereby allowing for straightforward heat transfer calculations in 2-D. No heat conduction is assumed to occur in the axial direction. The disadvantage is that no distinction between different regions is made within the unit cell and explicit fuel and graphite temperatures are not computed. This methodology was benchmarked for eight Fort Saint Vrain test fuel elements (Bradshaw et al, 1976). All but three test elements were found to operate at different power densities than the analytical estimates. The three elements with the same power were found to have average fuel temperatures close to their predicted values. Test element fuel temperatures were between 5 to 20°C higher than predicted over the test cycle life. Fuel performance, graphite structural and material properties, and fission product transport were also tested and benchmarked against analytical methods.

In the Fort Saint Vrain Test Element Safety Analysis Report, there was no mention of benchmarking of individual codes but rather only of the suite of codes. Thus, which codes or methods specifically performed better or worse than the others is unknown. Specifically, it is of interest whether 1-D flow modeling of coolant and bypass channels provides sufficient accuracy for convective heat transfer coefficient prediction. The issue of unit cell nodal heat transfer methods as compared to more detailed CFD was investigated in a study by Tak et al. (2008), which is discussed later. Other factors that contributed to the uncertainty of the reference calculations include: material property differences and fuel dimensional changes after irradiation.

Recent studies of HTGR core thermal hydraulics can be divided into two principal categories: core heat transfer, and reactor fluid flow. Computational results of recent thermal hydraulic studies are compared in the documented reactor design reports or experiments. In most cases, no experimental data are available to fully benchmark the results of a particular study; therefore, design results used are from the MHTGR, GT-MHR, NGNP (VHTR), or other reactor system. While most of the studies discussed assume consistent sets of key design parameters such as assembly block and fuel dimensions, there is significant variation in operational parameters such as inlet coolant temperature, core flow rate or desired average coolant outlet temperature, and core power. Graphite and fuel material properties can also be different depending on the author or study. Fortunately the assembly and fuel geometry is identical across all HTGR designs of interest.

2.1 Core Heat Transfer

Since the initial introduction of the proposed VHTR design based on the GT-MHR core, a thermal hydraulic and neutronic “point design” study was performed by INL (McDonald, 2003) in support of the NGNP. The goal of this analysis was to perform parametric sensitivity studies to establish a starting point for future analysis by

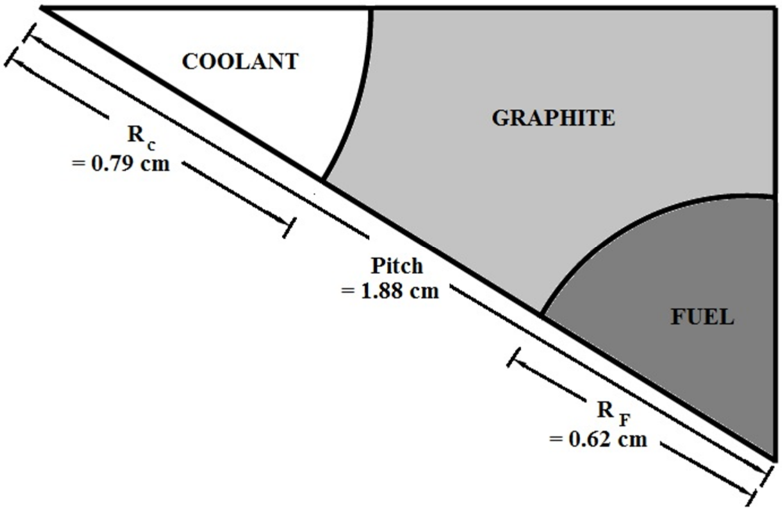

Figure 2.1 Triangular unit cell used by the steady state thermal hydraulic POKE code

quantifying the impact of variations to key design parameters such as core power, power density, assembly geometry, fuel configuration and others. Both steady state and transient, design basis accident, analyses were performed. In the INL study, McDonald assessed the impact on steady state, maximum core temperatures by varying bypass flow fractions, flow distribution and reactor power. The steady state method employed the POKE code to simulate one third of the core. The POKE code approximates core transfer using triangular unit cells, which includes one eighth of a coolant channel, one sixth of a fuel pin, and the adjoining graphite. Figure 2.1 presents a representative unit cell.

The core power profile was determined from Monte Carlo reactor physics calculations. The profile peaks in the lower portion due to control rod insertion to the critical location at the top of the reactor. The bypass and coolant flow distribution was fixed and not explicitly determined.

The first observation from the point design study is that maximum fuel temperatures increase when bypass flow is increased. Some design modifications that could reduce bypass flow include lateral core restraint mechanisms and a sealant between the core barrel and outer reflector gap to increase the resistance of that particular bypass flow path. The next observation from the point design is that maximum fuel temperatures could be reduced by 100°C if flow could be increased in hot coolant channels and decreased in channels next to lower power or cooler fuel compacts. Such precise flow control may be difficult to accomplish in practice. Finally it was found that increasing core power by adding active fuel blocks above the existing active core could be achieved without increasing maximum fuel temperatures. This was possible by adding two to four blocks on top of the existing ten block high core. Transient temperatures were not evaluated for these higher powers and may not be possible for the existing reactor vessel design, due to manufacturing size constraints or capital cost factors.

While these parametric studies revealed promising design modifications for the VHTR, a high degree of uncertainty remains due to the lack of explicit flow prediction and equivalent triangular unit cell modeling.

Since the NGNP point design study, there have been limited core heat transfer parametric design studies for HTGRs. One parametric core heat transfer study was conducted by Damian (2008) in support of the European Union RAPHAEL project (Futterer at al, 2006). The RAPHAEL conceptual design is similar to the GT-MHR with inlet and outlet temperatures of 490 and 850°C respectively. The 3-D thermal hydraulic code CAST3M and neutronics calculation scheme NEPHTIS were used to determine maximum fuel temperature for a peak assembly. Several fuel and assembly geometry configuration changes were investigated, but none were found to offer significant advantage over the originally proposed core assembly configuration. Reducing radial power peaking was found to be the most promising method for reducing peak fuel temperatures. Similar to the point design methodology, a coarse discretization of porous media homogenized cells formed the basis for core heat transfer calculations. Coolant channel and bypass flow were also fixed. Parameters such as bypass flow fraction, reflector material, power density, and control rod operation were varied to examine the impact on maximum fuel temperature. One novel observation was that replacing the outer graphite reflector with magnesium oxide (MgO) could reduce maximum transient fuel temperatures by 50°C due to the greater thermal mass ($\rho \times c_P$) of MgO compared to graphite.

In both studies, minimizing peaking was shown to reduce maximum fuel temperatures as compared to other methods such as minimizing bypass flow or altering fuel geometry. Power peaking is reduced by employing fuel management techniques that rotate blocks with higher fissile fuel content into lower power zones.

In addition to unit cell methods, CFD has also been used to analyze block or assembly level thermal hydraulics. The CFD code Trio_U was developed at CEA Grenoble to analyze partial helium channel blocking (Bieder and Graffard, 2008). The code was benchmarked against two PWR experiments UPTF and ROCOM designed for prediction of boron concentration during a boron injection event. The Trio_U code uses a hybrid finite volume finite element method for unstructured 3-D grids, and supports both RANS and LES modeling. Various RANS turbulence models can be used, including the standard k-ε model, k-ω based SST model, or a Reynolds stress model. Typical CFD runtimes for these PWR experiments range anywhere from 6 to 45 days on 32 to 64 processors.

In a study by Cinoi et al. (2006), the impact of helium channel blocking on maximum fuel temperatures was examined. Six standard fuel assemblies surrounding one “blocked” fuel assembly with 24 coolant channels having zero coolant flow were modeled. Imposed inlet and outlet temperatures of 500°C and 850°C, respectively were assumed. Maximum steady state fuel temperatures in the “blocked” assembly were found to reach 1925 °C. This exceeds the suggested temperature limit of 1600 °C for transient scenarios.

Unit cell and CFD methods are compared in detail in a study by Tak et al. (2008). The same triangular unit cell is compared to a CFD model for 1/12th of a standard fuel assembly. Inlet and outlet temperature conditions of 490°C and 950°C, respectively, were applied to the coolant channels. A flat power distribution was assumed for the axial length of the core. Bypass flow was calculated assuming a 1 mm reference gap. The maximum fuel temperature for the CFD case was found to be 1119°C. The similar unit cell model maximum temperature was found to be 1099°C. For cases with larger bypass gaps, CFD simulations indicate that maximum fuel temperatures could be up to 79°C higher than the triangular unit cell predictions. The main conclusion was that triangular unit cell methods can be safely applied to cases with low bypass flow. For cases with large bypass flow fractions, temperature gradients within the assembly block are not adequately calculated and thus maximum fuel temperatures are under predicted. A new unit cell that seeks to remedy this negative attribute of the triangular unit cell method by better estimating the intra-assembly heat conduction rates is presented in a subsequent section of this thesis.

2.2 Coolant Flow

Coolant in prismatic HTGRs enters at the base of the reactor vessel, flows upward through riser channels, collects in the upper plenum, and then travels downward through the core. Coolant is split between entering the active fuel assembly coolant channels and the gaps between assembly blocks. Predicting the fraction of total coolant flow that enters these gap region is complex and requires experimental validation.

In the spring of 2008, the Nuclear Regulatory Commission (US-NRC) Office of Nuclear Regulatory Research published a Phenomena Identification and Ranking Table (PIRT) on NGNP (VHTR) safety-relevant phenomena (Ball, 2008). Five expert panels were formed with individuals from various universities, national laboratories, reactor vendors and other industry sources. The panels were tasked with indentifying and ranking phenomena critical to both steady state and accident conditions. Thermal and fluid phenomena were divided into three categories: 1) factors affecting core cooling and coolant distribution, 2) factors affecting reactivity, power transients and power distribution, and 3) control of chemical attack and confinement of radioactivity. Core bypass flow was judged to be of high importance with a low or medium knowledge level. This means that more research is needed to measure bypass flow across the core, and to develop reactor analysis tools that can predict bypass flow. The PIRT highlights many issues with prediction and modeling of bypass flow. One of the modeling challenges is that since graphite changes physical shape under irradiation, bypass flow will vary axially along the core.

Argonne National Laboratory (ANL) performed core flow modeling and sensitivity studies for both the prismatic and pebble bed modular reactors (Lee et al, 2006), in support of uncertainty reduction for "beyond design basis" events as identified by the PIRT studies. Modeling of coolant flow in the core was based on a 2-D flow path and resistance network approach. Each fuel assembly was modeled as a single channel with additional channels for axial bypass flow and lateral cross flow between axially stacked assemblies. The conservation equations for mass and momentum are solved at each point using an assumed temperature profile based on the anticipated power profile predicted in the initial point design study. The objective was to identify flow paths that contribute to bypass flow the most. The vertical assembly gaps in the replaceable reflector region and near the permanent side reflector were identified as main bypass flow contributors. Cross flow was not found to play a substantial role in coolant flow distribution under normal operating conditions.

Recent CFD work, using the FLUENT code, by Sato et al. (2010) indicates that bypass flow is a complex phenomenon that is inherently coupled to neutronics, heat transfer, and fluid dynamics. Some discrepancies were documented when different turbulence models were used. The two most common models include: the standard k-ε model, and the Wilcox k-ω model. The k-ω predicted fuel temperatures 40 °C less than the k-ε model. It was suggested that these turbulence models need more verification against prismatic HTGR experiments. Another key insight was that radial power distribution had a larger effect on maximum fuel temperatures than axial power distribution. This result is investigated and described in the power perturbation studies conducted as part of this thesis work.

Experimental observation of VHTR coolant flow effects was first recorded for lower plenum mixing. Experiments and issues relating to hot streaking and maldistribution were presented by McEligot and McCreery (2004). It was postulated that lower plenum flow could be estimated by three different techniques: 1) using a representative liquid tank and dye injection method, 2) using a heated gas test section and thermal imaging camera, and 3) using a “Matched-Index-of-Refraction” (MIR) experiment where particle image velocimetry is employed to measure the fluid (mineral oil) velocity around the complex lower plenum structures constructed of quartz. Published results by McIlroy and McEligot (2010) describe the INL facility and setup for the MIR lower plenum fluid dynamics experiments. An approximately 1:7 scale model of a lower plenum “slice” near the reflector wall was constructed of clear fused quartz to match the index of refraction of the working fluid, mineral oil, so that optical measurement techniques could be employed.

The main benefit of the MIR experiments was providing sufficient data for CFD validation. A CFD analysis plan for the first standard problem for the VHTR is detailed in a study by Johnson (2008). The standard problem is based on the MIR lower plenum experiment. The CFD code FLUENT was selected for performing the computations because it was widely available to the U.S. NRC, national laboratories and other interested parties. Several questions that the CFD simulations were designed to address include whether 2D or 3D calculations are necessary for accurate flow prediction, if fine grids or coarse grids should be used, and what boundary conditions should be used. These questions are not only applicable to lower plenum flow modeling but also to full core coolant and bypass flow modeling.

To better predict the inlet conditions to the lower plenum, a RELAP model of the VHTR core was coupled to a CFD model of the lower plenum in a study by Anderson at al. (2008). The goal was to determine the degree of lower plenum mixing while using realistic inlet conditions supplied by RELAP analyses. Initially, a 44°C difference was observed at the RPV boundary but at the end of the pipe, the difference decreased to only 32°C. This was determined to be too high, as suggested limits for downstream components will likely be 20°C.

2.3 Summary and Path Forward

Thermal analyses of early HTGR designs often included a large suite of single function codes that employed a number of simplifications such as fixed flow fractions in coolant and bypass channels, 1/3rd fraction of whole core analysis, and neglected axial conduction. Triangular unit cells were commonly used where a fraction of fuel, graphite and coolant were homogenized. This method was found to be reasonably accurate for small bypass flow fractions but underestimated maximum fuel temperatures for larger fractions. The benefit of unit cell methods is computational efficiency. Fine mesh CFD methods are more accurate but have not been applied to the whole core due to computational cost. Some questions remain over what turbulence models and grid size should be used with CFD methods.

The goal of any new HTGR thermal hydraulic method should be to determine core temperature and fluid flow distributions that are both computationally efficient and can provide high fidelity results at any point in the core. Similar to the coupled lower plenum flow study by Anderson, some novel approaches such as coupling a systems analysis code such as RELAP for large core domains and CFD for local or detailed regions could be computationally efficient and provide accurate maximum fuel temperature and bypass flow predictions.

Another approach, described in more detail in the upcoming chapters, is to redevelop the unit cell method to adequately predict the axial and radial heat conduction within each assembly block. Together with a fluid coupling scheme, the whole core can be simulated. A high computational efficiency over CFD analyses is expected, because unit cell discretizations are larger than standard CFD meshes. This leads to fewer computations, and larger time-step sizes. The trade-off is that the temperature resolution at the assembly level is not as refined. For optimized or highly heterogeneous core configurations, having full core temperature and mass flow distributions would be more advantageous than having only a few regions of highly refined temperature profiles.

3. METHODOLOGY

The goal of this thesis work is to determine core temperature and fluid flow distributions during steady state conditions for the prismatic HTGR and analyze possible design variations. The steady state thermal hydraulic method can be divided into two parts: 1) core heat transfer, and 2) coolant flow. Core heat transfer is approximated by discretizing each assembly into unit cells, calculating the associated heat rates, and then integrating the energy balance over a time step. Coolant flow is approximated by modeling each coolant and bypass channel as a segmented 1-D channel, and using correlations for friction factor and Nusselt number for computing heat transfer rates.

The main benefit of this method is its ability for whole core analyses that explicitly determine bypass flow and account for graphite conduction within the assembly block. This leads to a high fidelity solution with less computational effort than similar CFD studies. This chapter describes the heat transfer and fluid models used to predict core-wide steady state temperature and mass flow distributions. The next chapter describes the numerical procedure and implementation details.

3.1 Core Heat Transfer Modeling

The prismatic HTGR reactor core consists of stacked hexagonal graphite assembly blocks with inner and outer reflector regions and a middle active core region as shown in Figure 3.1. Each fuel assembly has alternating fuel and coolant channels and is either a standard fuel assembly or a control fuel assembly with a single large hole reserved for a system shutdown or control rod. Both fuel assembly types are shown in Figure 3.2. Fuel and reflector assemblies also contain a central handling hole used to position blocks around the core. Burnable poison pins, which control reactivity over the fuel cycle, are placed on the corners of assemblies.

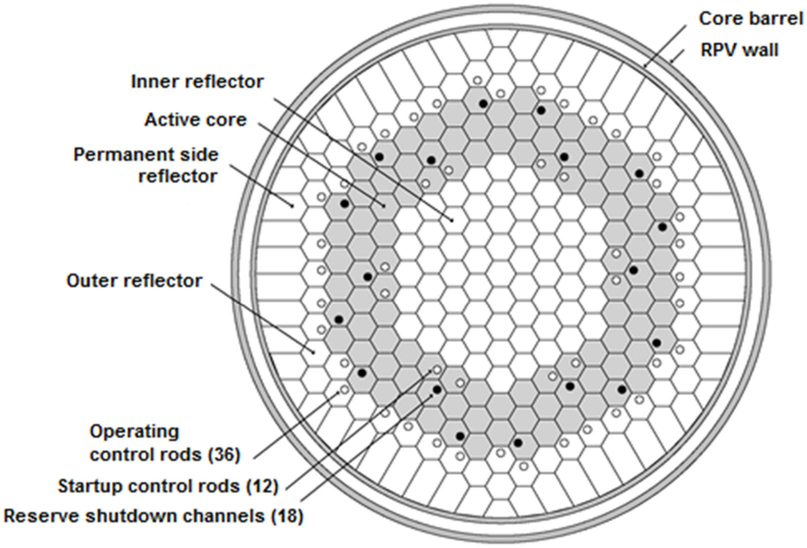

Figure 3.1 Example HTGR core axial slice

The unit cell method involves constructing local volume averaged energy balances, which are integrated to determine cell temperature. Each fuel assembly is discretized into unit cells with each cell containing either a fuel pin, coolant channel, or burnable poison pin. Each fuel pin is discretized in cylindrical geometry coordinates, assuming azimuthal symmetry. A gap exists between the fuel pin and the graphite block. The temperature of the graphite in the unit cell containing the fuel pin becomes the boundary condition for fuel pin unit cell heat conduction and radiation calculations. Likewise the assembly temperature of the graphite cell containing a coolant channel becomes the boundary condition for fluid heat transfer calculations. Unit cells containing burnable poison pins, a control rod hole, or the central handling hole are assumed to neither contribute nor remove heat from the assembly.

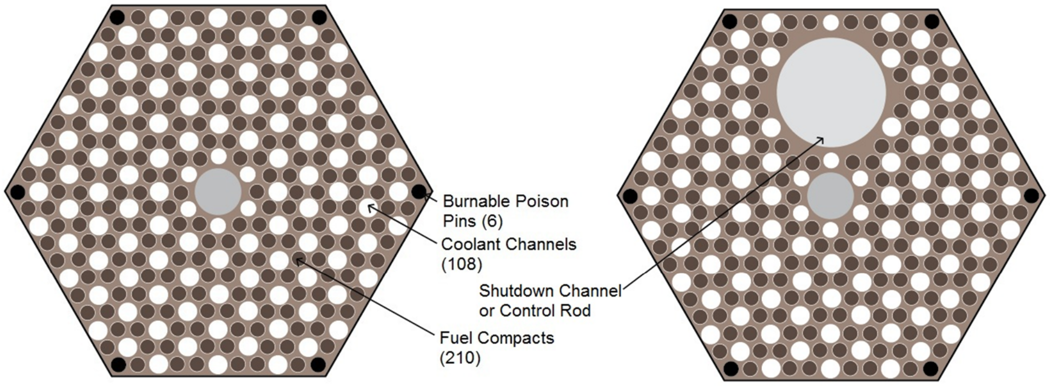

Figure 3.2 Prismatic HTGR standard fuel assembly (left) and control fuel assembly (right)

3.1.1 Unit Cell Energy Balance

The differential thermal energy equation within a graphite or cylindrical fuel cell is given by Eq. (3.1) where T is the temperature at some spatial point, t is time, $\mathbf{q}$ is heat flux, ρ is density, c_P is specific heat and q'''_{gen} is volumetric heat generation rate.

$$\rho c_P \frac{\partial T}{\partial t} = -\nabla \cdot \mathbf{q} + \mathrm{q}'''_{gen} \tag{3.1}$$

Integrating the energy equation over the unit cell volume, V, and applying the divergence theorem to the first term on the right hand side yields Eq. (3.2) where $\boldsymbol{n}$ is the outward normal to the unit cell surface.

$$\rho c_P \int_V \frac{\partial T}{\partial t} dV = -\int_S \mathbf{q} \cdot \mathbf{n} dS + \int_V \mathrm{q}'''_{gen} dV \tag{3.2}$$

Substituting the average unit cell temperature Eq. (3.3) and average volumetric heat generation rate yields Eq. (3.4).

$$T_{ave} = \frac{1}{V} \int T dV \tag{3.3}$$

$$\rho c_P \frac{\partial T_{ave}}{\partial t} = -\frac{1}{V} \int_S \mathbf{q} \cdot \mathbf{n} dS + \mathrm{q}'''_{gen,ave} \tag{3.4}$$

The surface integral can be represented as a summation over all the unit cell sides, which gives rise to Eq. (3.5) where $\mathbf{a}_s$ is the area of the cell surface "s" and $\mathbf{q}_i$ is the heat flux across that surface.

$$\rho c_P \frac{\partial T_{ave}}{\partial t} = -\frac{1}{V}\sum_{s=1}^{8} \mathbf{q}_s \cdot \mathbf{a}_s + \mathrm{q}'''_{gen,ave} \qquad (3.5)$$

For graphite unit cells, there are eight surfaces: 6 radial, and 2 axial. The heat flux for the neighboring unit cell, normal to that face, is not recomputed, but rather set to the inverse of the neighbor unit cell heat flux.

3.1.2 Geometry and Assembly Conduction

The heat flux across a cell face is determined by Fourier's law in 1-D as shown in Eq. (3.6) where the temperature gradient has been replaced with a first order finite difference approximation. The thermal conductivity is set to the geometric average for the two unit cells.

$$\mathbf{q}_i = -k_{ave}\frac{T_2 - T_1}{l} \qquad (3.6)$$

A typical unit cell containing a coolant channel is shown in Figure 3.3 with the relevant geometric terms highlighted. Geometric terms include the conduction length, l, cell surface areas, and cell volume. The conduction length is estimated as the distance from the average temperature location of the unit cell to the adjacent unit cell average temperature location. The average temperature location is based on the graphite center of mass of the unit cell.

The heat generation term for fuel unit cells is simply the power density. Heat input into graphite unit cells containing a fuel pin is a heat flux boundary condition based on fuel pin heat conduction.

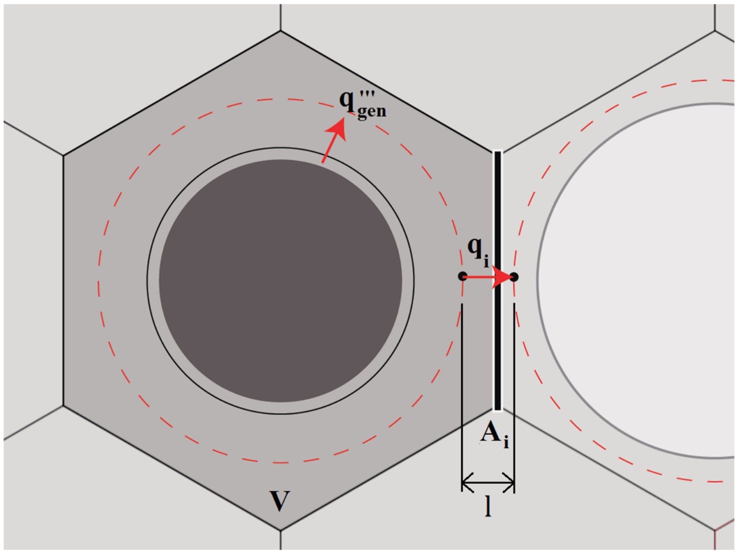

Figure 3.3 Graphite unit cell geometry

Graphite unit cells containing a coolant channel can have a heat removal or addition term based on the local convective heat transfer rate. Graphite assembly unit cells that are on the assembly perimeter contain an additional heat removal term due to bypass flow convection. Graphite unit cells containing a fuel compact are shown in Figure 3.4, while unit cells containing a coolant channel are shown in Figure 3.5.

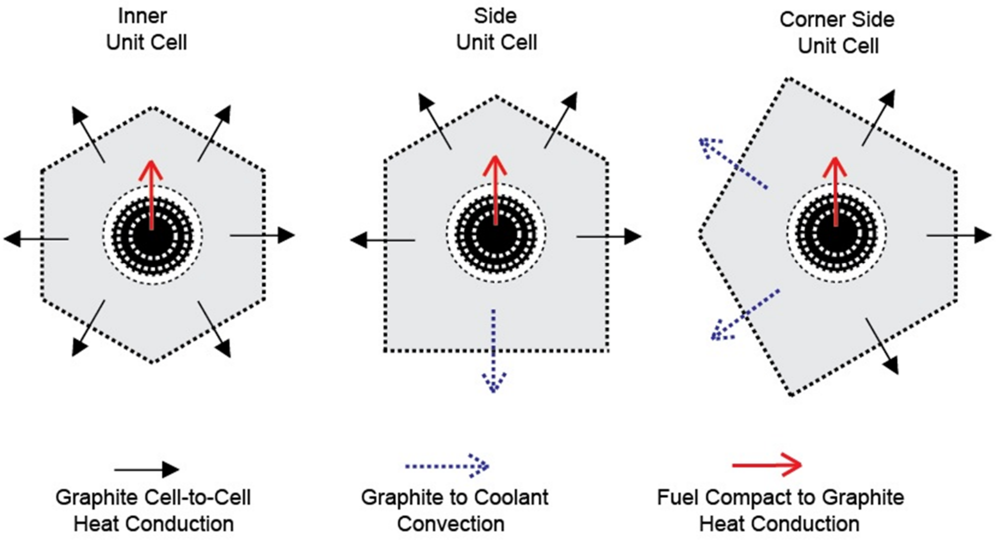

Figure 3.4 Different unit cells containing a fuel compact

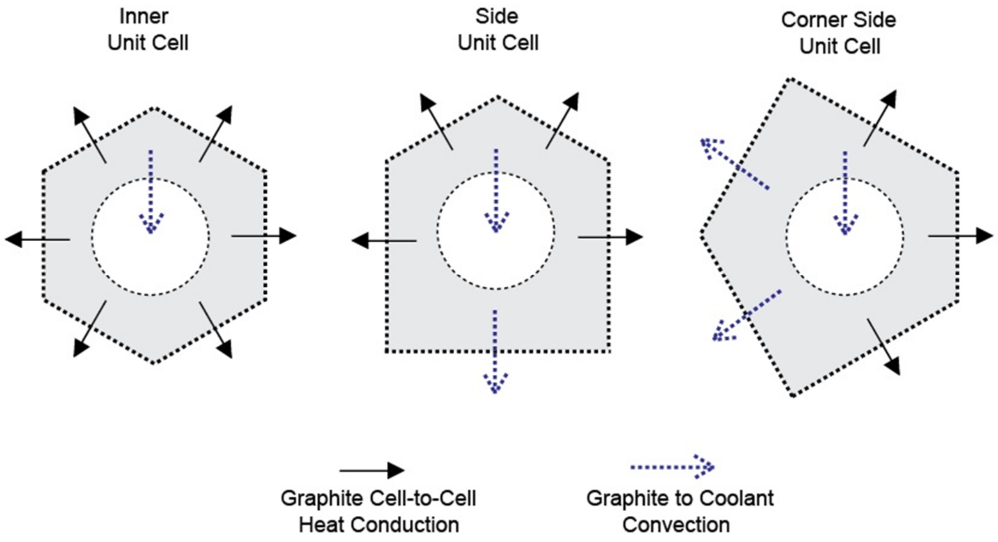

Figure 3.5 Different unit cells containing a coolant channel

Numerical values for the unit cell dimensions are shown in Figure 3.6. These dimensions are for assembly configurations exactly like that shown in Figure 3.3 and are easily computed using only the assembly flat-to-flat diameter, fuel compact-to-coolant channel pitch, and number of unit cells per assembly.

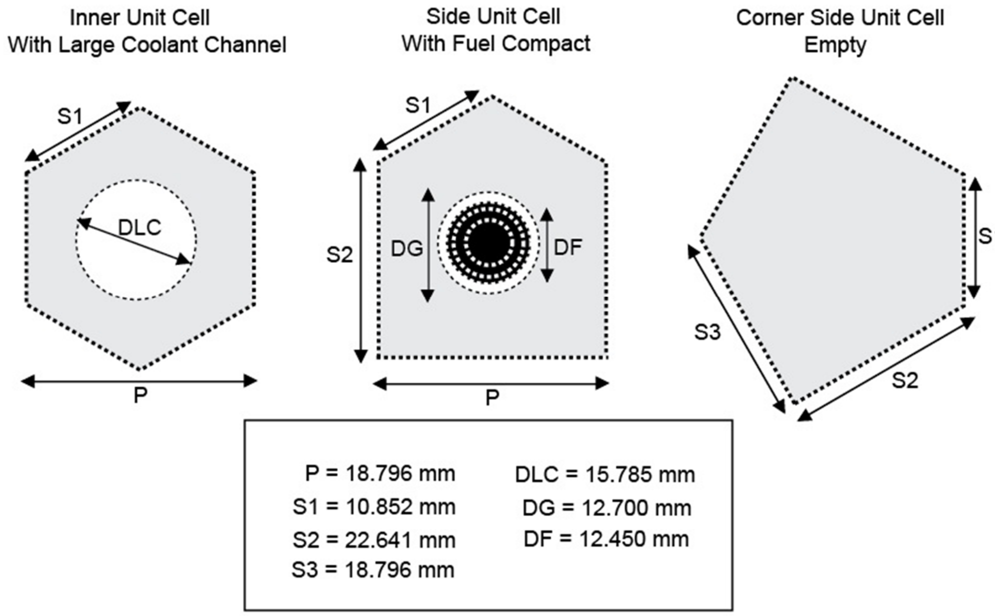

Figure 3.6 Unit cell dimensions for HTGR prismatic assemblies

3.1.3 Time Differencing and Stability

A first order explicit difference is used to model the time dependent term in the unit cell energy balance equation. The average unit cell temperature at the new time is denoted as $T_{ave}^{(2)}$ and the current average unit cell temperature is denoted as $T_{ave}^{(1)}$. Substituting the temperatures and time-step, Δt, into Eq. (3.5) and rearranging terms gives Eq. (3.7).

$$T_{ave}^{(2)} = T_{ave}^{(1)} + \frac{\Delta t}{\rho c_P} \cdot \left(\frac{1}{V} \sum_{s=1}^{8} q_s a_s + q'''_{gen} \right) \tag{3.7}$$

The time-step must be chosen small enough to ensure numerical stability, but very small time-steps may lead to long and impractical computation times. In Eq. (3.7), heat flux and heat generation are directly related to time-step size. For steady state analyses, heat generation is constant in time. Thus, numerical instability associated with assuming too large of a time-step size is most likely to occur early in the simulation when local heat flux values are greatest. Unit cell mass and heat capacity are inversely related to the maximum stable time-step size. Unit cell dimensions are then chosen by weighing the needs for computational speed, numerical stability, and detailed temperature prediction. The time-step sizes used for the GT-MHR and MHTGR analyses are 0.09 s and 0.05 s, respectively.

Determining the largest numerically stable time-step is more complex in this analysis than other computations that have a uniform grid or a single numerical procedure. One major reason is that, net conduction heat flux for any given unit cell is dependent on the temperature of all the neighboring unit cells. The limiting time-step is then time-dependent, and coupled to the entire domain. One example is at some specific point in time, a larger time-step for one cell that is numerically stable could cause an adjacent cell to become unstable. This view of just two cells is insufficient, because at some later point in time, a larger time-step could cause the previously stable unit cell to become unstable, while the unstable cell could be stable. The whole domain must therefore be considered. Another reason that it is difficult to pre-compute the limiting time-step is that convective heat removal is dependent on cell temperature. The channel mass flow, and thus convective heat removal, is also dependent on the flow dynamics of all of the other channels because of the connected inlet and outlet plenums. For a single time-step to be chosen at the start of computations, trial and error techniques must be used. One potential computational improvement to this will be discussed in the conclusions chapter.

Steady state is assumed to be achieved when global and local energy and heat transfer rates slow below a threshold value for a specified amount of simulation time. Specific convergence criteria are discussed in the next chapter.

3.2 Fluid Modeling

Helium coolant entering the prismatic core travels down three different types of flow paths. An example coolant flow path through the reactor vessel is shown in Figure 3.7. One path is the large core coolant channels that exist throughout the fuel assemblies. The other path is the smaller core coolant channels that exist only around the central handling hole and an extra channel above the control rod hole in fuel assemblies that replace a large coolant channel in standard fuel assemblies. Both of these coolant channel types are cylindrical with circular cross sections with forced turbulent flow during steady state operation. The final path is the bypass gaps surrounding each fuel and reflector assembly block. These gap channels are modeled as flat channels with forced turbulent flow. In lower core flow scenarios or for small bypass gaps the flow may be transitional or laminar.

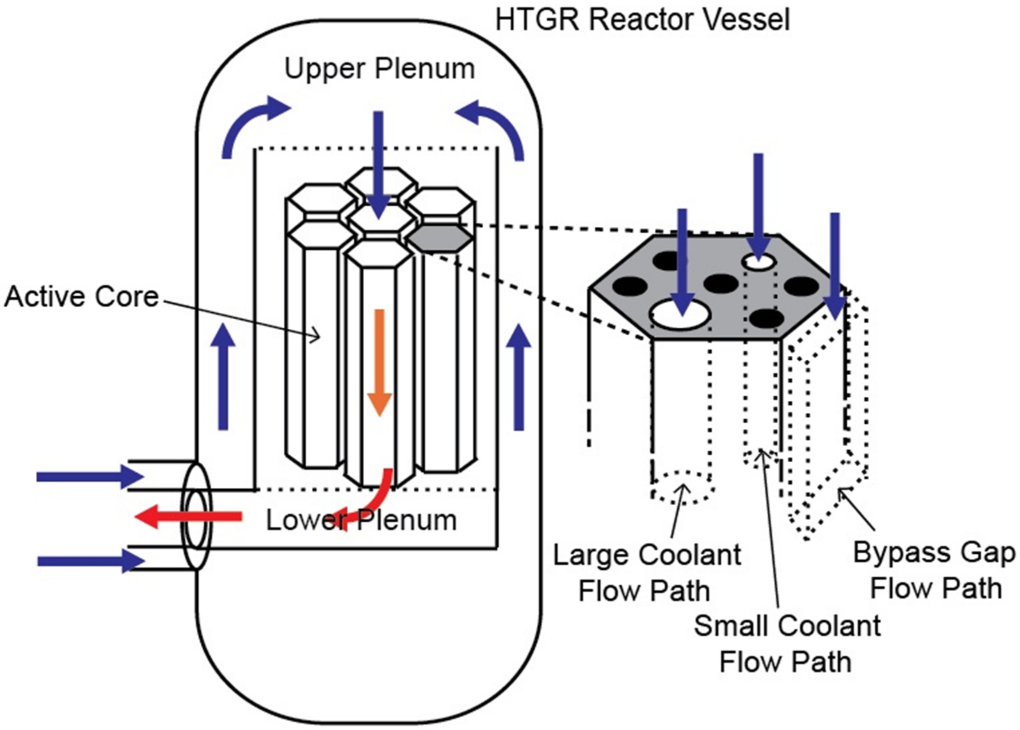

Figure 3.7 Example coolant flow paths through the vessel

For this analysis, the coolant is assumed to enter the active core region of the reactor vessel. Flow resistances associated with the inlet pipe, riser channels, upper and lower plenums are not modeled. In the active core, the flow through each channel experiences similar forces. The net pressure drop ($\Delta P = P_i - P_e$), where the exit pressure P_e is calculated from the fluid equations listed in Section 3.2.2, is assumed to result from the frictional and gravitational forces acting on the heated channels. Table 3.1 describes the physical and flow characteristics of each of the three flow path types. All helium flow characteristics (average coolant velocity, temperature, pressure) used in Table 3.1 are taken for GT-MHR inlet conditions specified in General Atomics (1996).

Table 3.1 Flow Path Characteristics by Type

Parameter	Large Coolant Channel	Small Coolant Channel	Bypass Gap Channel
Geometry	Circular	Circular	Flat Channel
D_H	15.8 mm	12.7 mm	6.0 mm
Area	197 mm^2	127 mm^2	600 mm^2
$\dot{m}^*$	0.0192 kg/s	0.0105 kg/s	0.0400 kg/s
Re*	40100	27220	10370

* Helium thermal properties computed at 490°C

The purpose of flow modeling is to determine the heat removal rate in the core and to determine the specific mass flow rates for each channel or bypass gap. Each channel is modeled as 1-D flow in the axial direction. Axial discretization is selected to match the core unit cell axial discretization. For both the GT-MHR and MHTGR analyses, the core height is 7.93 m and ten axial nodes are selected; therefore, the axial height of each unit cell is 0.793 m. The same axial discretization is chosen for the fluid channel. Thus, the wall temperature for convective heat transfer calculations is the graphite unit cell temperature. The basic procedure is to choose an initial guess mass flow rate for the channel, apply correlations for friction factor and Nusselt number assuming uniform wall heat flux boundary conditions, determine the outlet fluid flow characteristics, and then scale the inlet mass flow rates accordingly so that the exit pressure across all the channels is the same.

3.2.1 Wall friction and Nusselt Correlations

The active core height (coolant channel length) for both the MHTGR and GT-MHR is 7.9 meters. The fluid entrance length for a large coolant channel, using an integral turbulent boundary layer analysis relationship by Zhi-qing (1982) and the parameters in Table 3.1, is 0.3 meters.

$$l_{ent,hy} = 1.359 D_H \operatorname{Re}_{D_H}^{0.25} = 1.359(0.0158)(40100)^{0.25} \approx 0.3 \tag{3.8}$$

The thermal entrance length can be approximated by multiplying the hydrodynamic boundary layer by the fluid Prandtl number. Helium has a Prandtl number of approximately 0.65 at 490°C, thus the thermal entrance length is shorter than the hydrodynamic length. Because both entrance lengths are much smaller than the channel length, the assumption is made that the fluid is fully developed over the entire channel length.

Because the Reynolds numbers for all the channel types listed in Table 3.1, are greater than 2000, turbulent flow is assumed. For internal turbulent flow in a circular pipe, the friction factor correlation by Churchill (1977) is used, as shown in Eq. (3.9).

$$\begin{gathered} f = 8\left[\left(\frac{8}{\operatorname{Re}_{D_H}}\right)^{12} + \frac{1}{\left(A+B\right)^{3/2}}\right]^{1/12} \\ A = \left\{2.457\ln\left(\frac{1}{\left(\frac{7}{\operatorname{Re}_{D_H}}\right)^{0.9} + 0.27\frac{\varepsilon_s}{D_H}}\right)\right\}^{16}, \quad B = \left\{\frac{37,530}{\operatorname{Re}_{D_H}}\right\}^{16} \end{gathered} \tag{3.9}$$

Surface roughness is denoted by ε_s, and for graphite it is estimated to be $10\,\mu m$.

The convective heat transfer coefficient is estimated from the Dittus and Boelter correlation, as shown in Eq. (3.10).

$$Nu_{D_H} = \frac{hD_H}{k} = 0.023 \operatorname{Re}_{D_H}^{0.8} \operatorname{Pr}^{0.4} \tag{3.10}$$

3.2.2 Channel mass flow iteration procedure

For each cell, the inlet fluid temperature and pressure is used as an approximation to obtain all the relevant fluid properties used in the correlations. The outlet temperature is then computed and an average temperature is used for correlations. Iterations are then performed until the outlet temperature and fluid properties converge. This usually occurs after three to four iterations, for an outlet temperature convergence of less than 0.1°C between iterations.

An estimate of convective heat removal Q_{conv} is made based on the convective heat transfer coefficient. Using the estimates for velocity, friction factor, and Q_{conv} the governing equations are solved for each axial node. The governing equations include conservation of mass, momentum, energy, and the ideal gas law, which are shown below in Eq. (3.11) through (3.14). Subscript i denotes the inlet property and subscript e denotes the exit property. The average velocity between the inlet and exit is denoted as v_{ave}. The four equation linear system is solved for the four unknowns: ρ_e, v_e, T_e, and P_e.

$$\rho_i v_i = \rho_e v_e \tag{3.11}$$

$$\left(\frac{P_i}{\rho_i} + \frac{v_i^2}{2} + gz_i\right) - \left(\frac{P_e}{\rho_e} + \frac{v_e^2}{2} + gz_e\right) = f\,\frac{L}{D_H}\frac{v_{ave}^2}{2} \tag{3.12}$$

$$Q_{conv} = \dot{m}c_p\left(T_e - T_i\right) \tag{3.13}$$

$$P_e = \rho_e R T_e \tag{3.14}$$

After the exit pressure is determined for each channel, a linear relationship can be formed for pressure drop as a function of channel mass flow rate. Eq (3.15) and Eq. (3.16) show the linear relationship for the same channel but for two different inlet mass flow rates denoted by the superscript iteration number. The subscript, n, denotes the channel number.

$$\Delta P_n^{(0)} = A_n + B_n \dot{m}_n^{(0)} \tag{3.15}$$

$$\Delta P_n^{(1)} = A_n + B_n \dot{m}_n^{(1)} \tag{3.16}$$

Constants A_n and B_n can be determined by solving the simple two equation linear system above. The updated pressure drop is constrained to be identical for each channel because at steady state, the inlet pressure and outlet pressure are assumed to be uniform radially across the core. The updated pressure drop is denoted as $\Delta P_n^{(2)}$. The updated channel mass flow rate is denoted as $\dot{m}_n^{(2)}$. The linear relationship can be rearranged and then added together with all the channels as shown in Eq. (3.17).

$$\sum_{n=1}^{N} \frac{\Delta P^{(2)}}{B_n} = \sum_{n=1}^{N} \left(\frac{A_n}{B_n} + \dot{m}_n^{(2)} \right) \tag{3.17}$$

The updated pressure drop can be determined directly now because the summation of all the new mass flow rates is the total core flow $\left(\sum_{n=1}^{N} \dot{m}_n = \dot{m}_{tot} \right)$ and the pressure drop for each channel is assumed to be identical $\left(\Delta P_1^{(2)} = \Delta P_2^{(2)} = \ldots = \Delta P_n^{(2)} = \ldots = \Delta P_N^{(2)} \right)$ and is shown below in Eq. (3.18).

$$\Delta P^{(2)} = \frac{\dot{m}_{tot} + \sum_{n=1}^{N} \frac{A_n}{B_n}}{\sum_{n=1}^{N} \frac{1}{B_n}} \tag{3.18}$$

The updated iteration mass flow rate for each channel can now be determined by substituting Eq. (3.18) back into its linear relationship. The new iteration mass flow rate is shown below in Eq. (3.19).

$$\dot{m}_n^{(2)} = \frac{\Delta P^{(2)} - A_n}{B_n} \tag{3.19}$$

The procedure repeats using the updated mass flow rate until pressure drop is adequately uniform across all the channels. The pressure drop is assumed to be uniform when it is within 1 Pa of each channel. The linear constants A_n and B_n are recomputed for each successive iteration after $\dot{m}_n^{(2)}$ is determined. To perform as few iterations as possible, the previous two mass flow rate distributions (at time $t = t_{i-2}$ and $t = t_{i-1}$) are used to determine $\Delta P^{(0)}$ and $\Delta P^{(1)}$ at the start of each new core heat transfer time-step (at time $t = t_i$).

Numerical instability could occur if too many iterations are performed and the new mass flow rate is identical to the value from the previous iteration. This leads to B_n approaching infinity or returning NaN (not-a-number) errors. Another instability that occurs is if the linear approximation overestimates the new pressure drop. This leads to some channels having negative mass flow rates with others having larger than normal values. These instabilities can be easily identified and rectified with appropriate logic in the computational scheme. The simplest logic implementation to prevent instability is to terminate the iteration procedure and use the last stable mass flow rate distribution for the current time-step mass flow rate distribution. This causes the pressure drop to not converge to the 1 Pa limit for each channel but rather is typically between $1 < Pa < 10$. If the convergence criterion was set higher, to 10 Pa, then no iteration would be needed because the last time-step mass flow distribution satisfies the criterion for the current time-step. This is only performed at the start of the simulation, as wall temperature conditions are rapidly changing, and instability is more likely to occur.

The method used to compute flow rates and distributions here is different than the RELAP and CFD analyses discussed in the literature review, in that each coolant and bypass channel is modeled and a complete mass flow distribution can be obtained using the present approach. Similar to CFD analyses, only a total or overall mass flow rate is needed to solve for the mass flow rate for each channel. The surrounding graphite wall temperature is assumed to be the graphite unit cell temperature.

Thermal fluid properties for graphite, helium, and fuel compact material used here are taken from an INL report (Johnson et al, 2009).

The next chapter discusses the computational approach for implementing the thermal-fluid analysis method described in this chapter.

4. COMPUTATIONAL SCHEME

In this chapter, the methods presented in the previous chapter are outlined in detail as a computational scheme. The methodology presented in the previous chapter is primarily developed using the Fortran 95 programming language with elements of modern Fortran or Fortran 2003. Linking and compiling of the computer code was performed using the GNU Fortran (GFortran) compiler package version 4.6.2. Testing and execution were performed on the Georgia Tech NRE SCYLD cluster and the Georgia Tech PACE-FoRCE cluster.

The general procedure is illustrated in Figure 4.1. The first phase is to read input files, allocate array sizes based on input parameters, initialize constant values and determine if the simulation is a restart of an earlier execution or a new steady state run with an arbitrary initial temperature distribution. The next phase is to perform the heat

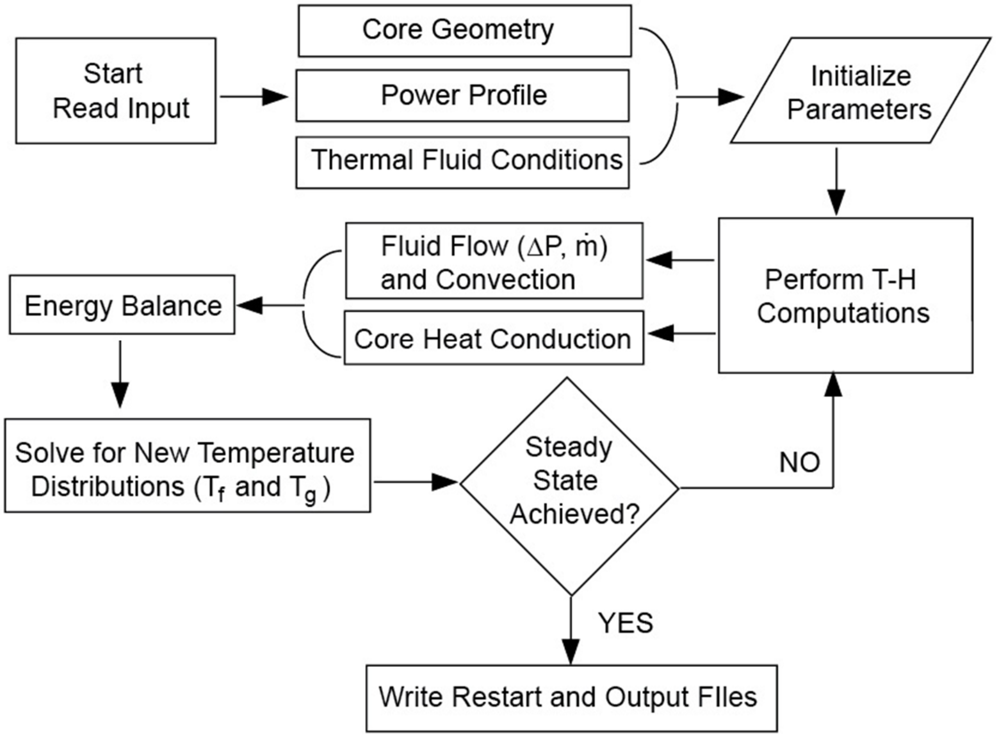

Figure 4.1 Thermal hydraulic computational scheme

transfer and fluid calculations at each time-step. The final phase is to determine if steady state is achieved or if the simulation should be restarted later to achieve steady state. In either case, output files are written so the code may be executed again.

4.1 Initialization

Two files are opened upon code execution. The first input file (parameter file) contains the geometry, spatial and time discretization for the problem. The second file (power file) contains the pin-powers for every fuel pin in the core. The pin-powers can be supplied by the user, for example a flat power profile, or by a coupled neutronics code. After reading the input files, assembly and core geometry is initialized. The 1-D fluid node network is constructed based on the location of coolant channels within each assembly and the total number of assembly blocks. Before the central thermal hydraulic computations commence, restart files are executed and initial temperature and heat flux values are applied.

4.1.1 Input and Restart Files

Time discretization terms in the parameter file include: the maximum simulation time, time-step size, and output frequency. Spatial discretization terms include: number of axial divisions, number of radial fuel pin divisions, and number of assembly unit cells per axial division. Specific geometry, time, and spatial discretization values will are provided in the next chapter for two different reactor types.

Comprehensive data sets called restart files are written at a user defined frequency. Restart files contain every fuel, graphite and coolant temperature, channel mass flow and pressure at every axial division, simulation time, and heat rates for the current time-step. This allows for the simulation to be interrupted and then continued at some later point with no loss in computational effort.

4.1.2 Geometry Initialization

Assemblies and unit cells within each assembly need two identification numbers to link heat conduction and heat removal. Figure 4.2 illustrates an example core and assembly configuration. The "AN" refers to the assembly location number and "AT" refers to the assembly type. The "CN" refers to the unit cell location number and "CT" refers to the unit cell type. This example assumes that there are seven assemblies each with 19 unit cells. Assembly types 1, 2, and 3 correspond to graphite reflector, standard fuel assembly, and fuel assembly with control rod respectively. Unit cell types 1, 2, and 3 correspond to fuel pin, coolant channel, and solid graphite respectively. The numbering scheme for the core starts with the innermost assembly, and then works outward and clockwise starting with the top assembly. The numbering scheme for the unit cells starts in the upper left corner of the assembly and works left to right and downward. In the next chapter, specific numbering is described for the GT-MHR and MHTGR cores.

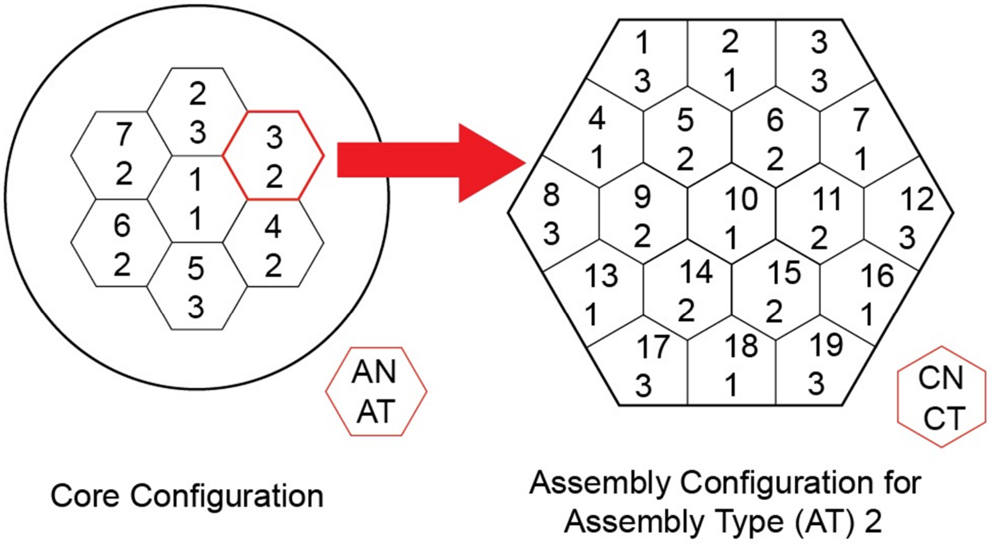

Figure 4.2 Example assembly and unit cell identification scheme

The location numbers “AN” (assembly number) and “CN” (cell number) are used to determine the adjacent neighboring cells or assemblies for inter-cell or inter-assembly heat conduction. The type numbers “AT” (assembly type) and “CT” (cell type) specify whether heat generation from fuel pins or heat removal from coolant channels occur within that cell or assembly.

4.2 Thermal Hydraulic Iteration Procedure

The first process that occurs is reading the input files and initializing the assembly and core geometry. Once an initial temperature distribution is applied by either user input or from restart files, the outer most time-step iteration loop begins. Three heat transfer rates are needed for every unit cell in the core. The first rate is the convective heat removal rate. The second is the heat generation rate, which at steady state is a constant and is not recomputed at each time-step. The heat generation rate is provided by the user, in the pin power input file. Finally, the total heat conduction rate out of or in to each unit cell is needed. These rates are then combined and the net energy increase or decrease is determined. Assuming a constant specific heat and density during that time-step, the new average unit cell temperature is found.

4.2.1. 1-D Coolant Flow and Mass Flow Iterations

Convective heat transfer rates for unit cells containing a coolant channel or on the assembly boundary next to a bypass gap are determined from correlations, given the channel inlet mass flow rate and temperature. Channel exit pressures are determined for two different trial inlet mass flow rates. The new guess for channel mass flow rate distribution is determined by a linear extrapolation, or interpolation, using two prior mass flow rate distributions and by matching the pressure drop for the other channels. The trial inlet mass flow rates are chosen to be near the predicted value to ensure the least number of iterations are performed. Successive mass flow rate distribution predictions use the most recent mass flow rate distribution and pressure drop information to perform new mass flow rate extrapolations. Convergence is said to occur when a uniform pressure drop across all the channels is achieved (normally < 1 Pa).

The mass flow rate distribution is updated at each time-step. The most recent mass flow rate distributions from the previous time step are used at each new time-step for extrapolation data. The maximum number of mass flow iterations required to achieve convergence occurs during the first core thermal hydraulic time step because the trial extrapolation data are arbitrary and not based on previous time-steps.

The channel exit pressure is found by performing the procedure outlined in Figure 4.3. Inlet fluid properties are known from the steady state reactor design parameters. Outlet conditions are estimated and verified once the exit temperature and pressure are determined. If the outlet temperature yields an average node temperature different than what is assumed for estimating the convective heat rate, then iteration is necessary to achieve convergence on the exit fluid properties.

4.2.2 Core Heat Transfer Iterations

Once the convective heat rates are determined for each cell, heat conduction rates are calculated. The average graphite unit cell temperature and the average graphite unit cell temperatures of all eight neighbors are used in Eq. 6 to determine the eight different heat conduction rates associated with that particular unit cell. For unit cells that lie on an assembly boundary, only six conduction rates are calculated (four radial, two axial). For unit cells that lie on an assembly corner, only five conduction rates are calculated (three radial, two axial). For unit cells that are on the top or bottom axial layer, one less conduction rate is determined due to an assumed insulating boundary condition.

For steady state simulations, the heat generation rate is assumed to be constant. Once all rates are known, the new graphite unit cell temperature is determined from Eq. (3.7). The procedure is then repeated for the next time step.

Output is checked for the first few iterations, when heat transfer rates are the highest, to verify that the time-step size does not cause numerical instability. Key energy balance output parameters include: total convective heat removal rate, total core graphite heat-up/cooling rate, and total core fuel heat-up/cooling rate. These parameters will sum exactly to the total heat generation rate within machine precision. If at any iteration they do not, this indicates that the time-step is too large and should be reduced to achieve numerical stability.

Convergence is assumed to occur when the graphite and fuel sensible heating rates are sufficiently close to zero, and convective heat removal equals the heat generation rate. All simulations performed here were run for 8,000 to 10,000 simulation seconds with a time-step size between 0.05 and 0.09 seconds. After this time, total convective heat removal rates were within 0.1% of the heat generation rate.

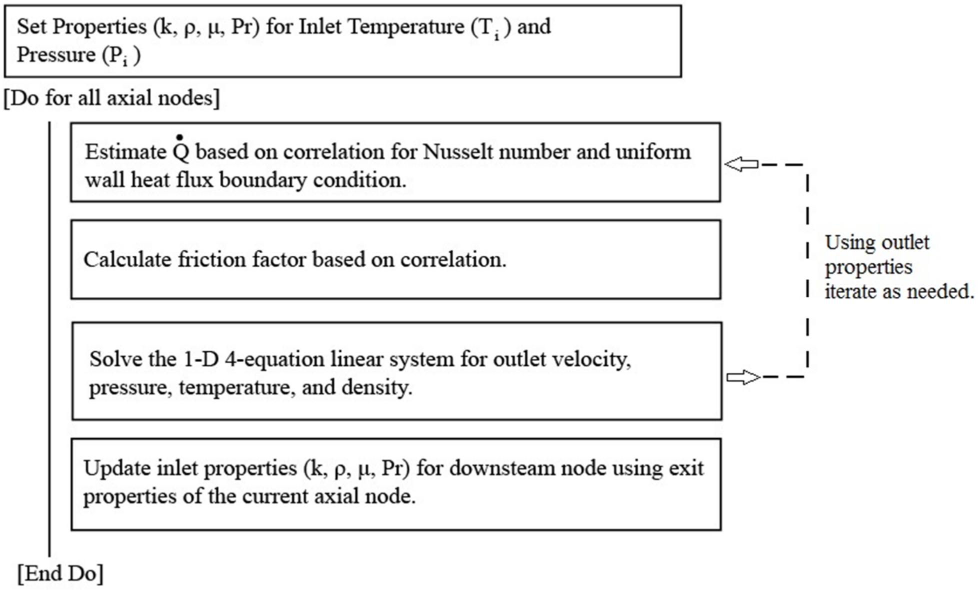

Figure 4.3 Channel fluid properties and pressure drop pseudocode

5. RESULTS

Full core, steady state simulations with uniform axial and radial power profiles, for both the MHTGR and GT-MHR are presented in this section. Comparisons between the two designs are discussed. Temperature plots as well as tables for both designs are included, which document important thermal hydraulic factors such as average and peak fuel temperatures. Mass flow distributions are also included to illustrate the impact of bypass gap width and the coolant channel dimensions. Numerical considerations such as time-step size, number of iterations, and initial conditions are described with their impact on computational performance and accuracy. Finally, a brief set of parametric studies is included to quantify the effect that some core design factors have on thermal hydraulic analysis.

5.1 MHTGR Steady State

The MHTGR steady state simulation was initiated assuming a uniform power distribution. The initial core temperature distribution was set to an axially and radially uniform profile equal to the coolant inlet temperature. The choice of initial temperature distribution is arbitrary so long as it is within the expected range of operating temperatures. An initial coolant velocity of 28.5 ms^{-1} was chosen for fluid model initialization. This an average velocity based on the total mass flow rate, core flow area, and inlet density. During the first core time step, the fluid model performs 6 iterations to converge individual channel mass flow rates. The total steady state simulation took 33.4 hours to execute on eight AMD, 64-bit, 3.0 GHz processors. The simulation was run for 10,000 seconds with a time-step of 0.06 seconds for a total of 166,667 iterations. Intermediate time-step sizes, for late simulation times, were not used. Restart files were written every 833 iterations or every 50 seconds of simulation time.

The simulation time of 10,000 seconds was chosen to ensure temperature convergence. Total core heat removal rate approaches 1% of the design value within 3,250 seconds. Core fuel temperatures after 4,200 seconds are within 1°C of their final values after 10,000 seconds. Graphite temperatures are within 1°C of their final values after 5,600 seconds. As steady state is approached, heat removal approaches heat generation and both the fuel and graphite sensible heat change approaches zero. The change in fuel and graphite sensible heat is plotted along with the core heat generation and removal rates for the first 500 seconds of simulation time in Figure 5.1.

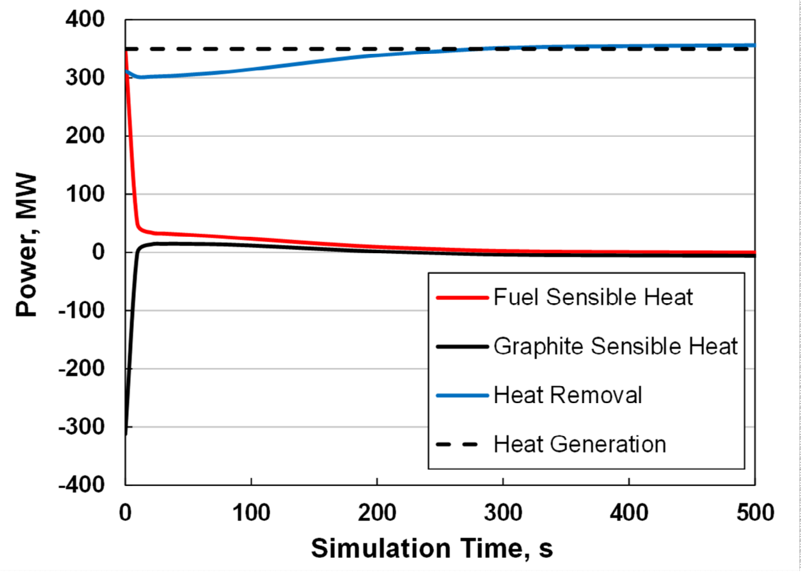

Figure 5.1 MHTGR components of core energy balance for the first 500 seconds

During the first time-step, the fuel temperature is assumed to be equal to the graphite temperature. This results in a large increase in fuel temperatures. During the first time-step, graphite temperatures rapidly decrease as only convective heat removal occurs. After 10 seconds, both fuel and graphite temperature changes decrease. After about 250 seconds, graphite temperatures begin to stabilize.

Final steady state, 3-D core temperature distributions for the fuel, graphite and coolant are shown in Figures 5.2, 5.3, and 5.4 respectively. In Figure 5.2, the fuel compact centerline or maximum temperature is shown. In Figure 5.4, only the coolant channel temperatures are shown. The bypass gap temperature is within 1 to 5°C of the adjacent graphite temperature.

The inner and outer reflector blocks throughout the core remain close to the inlet helium temperature of 259°C. Bypass flow (without any heat generation) in these regions, causes a nearly constant axial temperature profile. Near the bottom of the core, some heat conduction outside of the active core occurs, which slightly raises the graphite temperature.

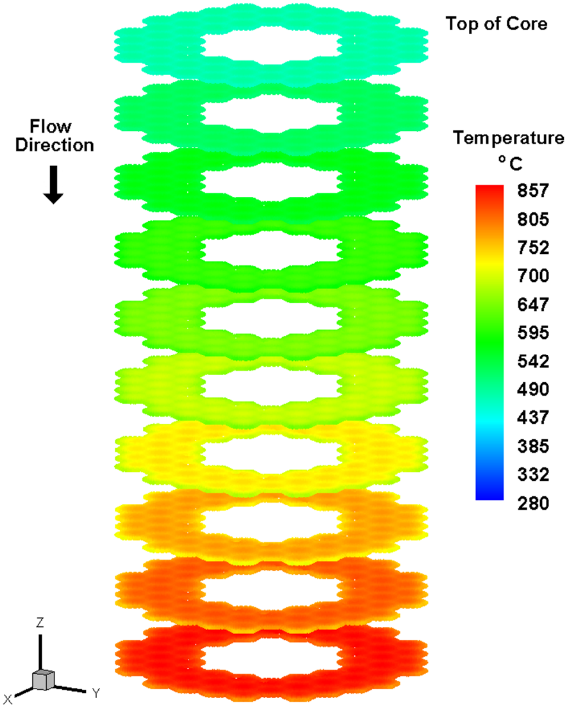

Figure 5.2 Fuel MHTGR base-case, 3-D core temperature plot

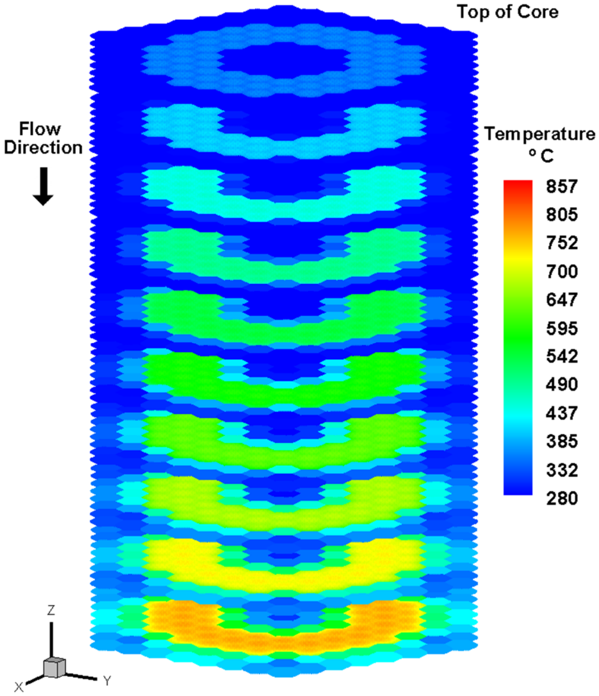

Figure 5.3 Graphite MHTGR base-case, 3-D core temperature plot

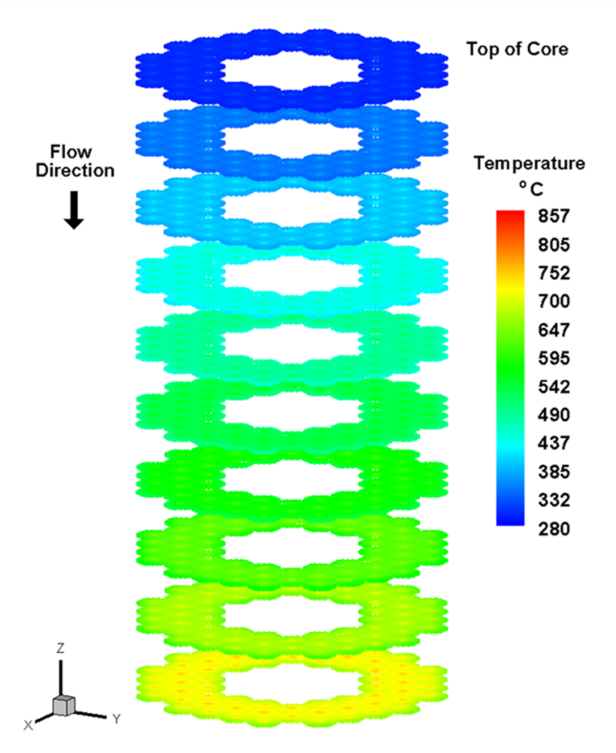

Figure 5.4 Coolant MHTGR base-case, 3-D core temperature plot

In the active fuel region, the graphite temperature follows the fuel temperature profile. Bypass flow around each active assembly side lowers the graphite periphery temperature. For a uniform power generation, at any core elevation, the temperature difference between the fuel and graphite is relatively constant. The temperature difference is slightly higher at the top of the core due to axial fuel conduction. The temperature difference, at any core elevation, is between 82°C and 120°C. In this analysis, axial fuel conduction may be overestimated due to several factors. The fuel is modeled as a single continuous fuel rod, when physically; the fuel compacts are discontinuous at the axial block interfaces. There is also a small graphite seal between each block that holds the compacts within the blocks. Graphite block radial placement may also offset the fuel compact placement in the axial direction. Nevertheless, hot temperature spots directly above and below the fuel compacts will drive some axial heat conduction. There also may be some radial bypass cross flow that could introduce a heat removal mechanism, which would reduce heat axial heat conduction. These complex factors are beyond the scope of this analysis and are not modeled.

The coolant temperature profile follows the graphite temperature profile which defines the wall temperature for convective heat removal. The coolant temperature is hottest in the center of each assembly due to higher graphite temperatures, and due to the six smaller diameter channels, which have higher local convective heat transfer coefficients. An axial temperature plot for the uniform power base-case is included in Section 5.3. Maximum and average core temperatures are provided in Table 5.1. Average temperatures are determined by performing a mass weighted average of all the graphite, fuel, and coolant unit cells.

Table 5.1 MHTGR base-case core temperatures

Material	Peak Temperature, [°C]	Average Temperature, [°C]
Fuel	861.6	639.5
Graphite	771.3	375.7
Coolant	740.1	503.6

For a bypass gap width of 3.12 mm, bypass flow around each assembly block accounts for 10.6% of the total coolant flow while only accounting for 7.8% of the total heat removal. This heat removal comes primarily from the active fuel assembly sides. At steady state, heat removal in the reflector block regions is negligible. The impact of bypass flow on fuel and graphite temperatures is discussed in Section 5.3.

The helium enters at the base of the vessel, travels upward along the vessel wall, collects in the upper plenum, and then flows downward through the core. The flow paths through the core include large coolant channels, small coolant channels, and assembly bypass gaps between each hexagonal block. The pressure drop between the top and bottom of the active core is 17.3 kPa. Core pressure drop accounts for the friction, thermal expansion, and gravitational contributions. Bypass gap width and total core flow rate are found to significantly affect core pressure drop. Entrance, exit, and other minor losses are not computed. A plot of the helium mass flux is shown in Figure 5.5.

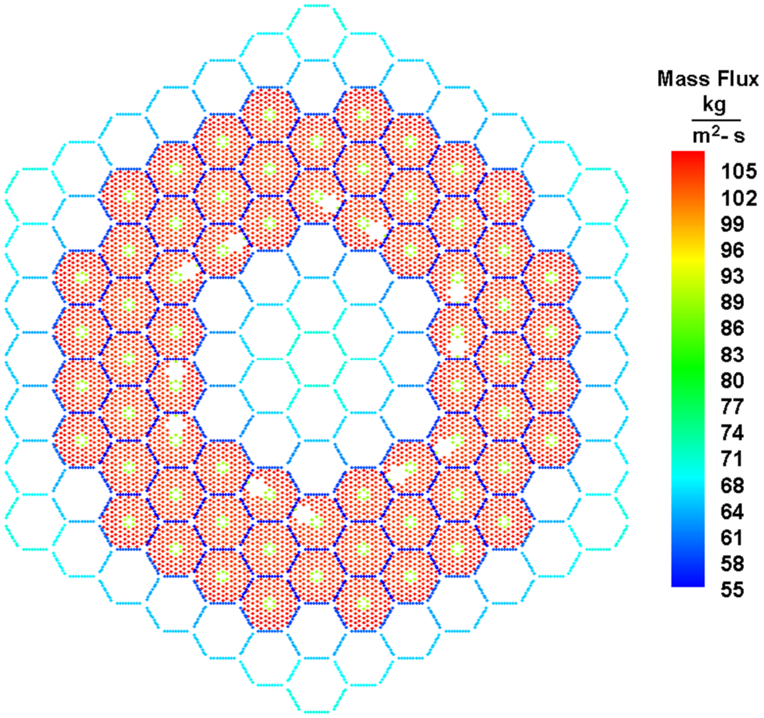

Figure 5.5 MHTGR base-case mass flux distribution

Bypass gap channels outside of the core region have higher mass flow rates due to lower temperature helium, which has a higher density than in the core region. The density of helium at 6.39 MPa, at temperatures of 430°C and 730°C is 4.33 kg/m^3 and 3.04 kg/m^3 respectively. The mass flux ratio is about the same as the channel exit density ratio, 1.35 and 1.42 respectively. The six small diameter coolant channels in the center of the assembly also have lower mass flux values than in the large diameter channels. This can also be attributed primarily to temperature/density differences.

5.2 GT-MHR Steady State and Comparison

The GT-MHR steady state simulation was executed with a slightly higher initial temperature distribution than the MHTGR, due to the higher coolant inlet temperature of 490°C for the GT-MHR compared to 260°C for the MHTGR. The temperature and power were also both uniform in the axial and radial directions. The choice of the initial temperature distribution is arbitrary; however, it can affect the total computation time and numerical stability if non-physical conduction heat fluxes result from such assumptions. The initial fluid velocity is 32 ms^{-1} and is slightly higher than in the MHTGR because it has a greater total core flow rate. Similarly, the choice of initial fluid velocity is arbitrary; however, it must be reasonably accurate to ensure numerical stability. The simulation was run for 10,000 seconds with a time-step of 0.09 seconds for a total of 111,112 iterations. The GT-MHR, using a similar set of numerical parameters and computer hardware, took 35.3 hours to reach steady state. The larger GT-MHR core, with fewer iterations, took 1.9 hours longer to compute than the MHTGR. A larger time-step was chosen by trial and error. As discussed in the time-differencing and stability section, the choice of time-step is complex and theoretically time-dependent.

Fuel sensible heating, graphite sensible heating, and convective heat removal for the first 500 seconds exhibit similar behavior as for the MHTGR. Total core heat removal is within 1% of the design value after 3335 seconds. Fuel and graphite temperatures are within 1% of their final values after 5100 seconds.

Final steady state, 3-D core temperature distributions for the fuel, graphite and coolant are shown in Figures 5.6, 5.7 and 5.8 respectively.

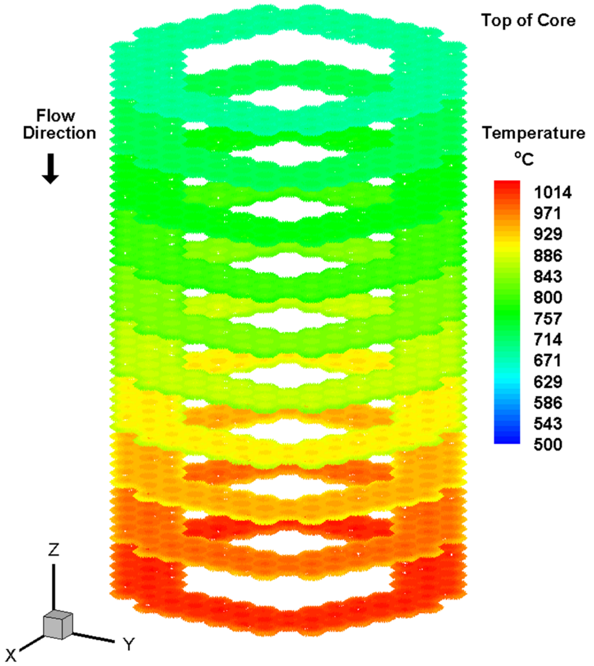

Figure 5.6 Fuel GT-MHR base-case, 3-D core temperature plot

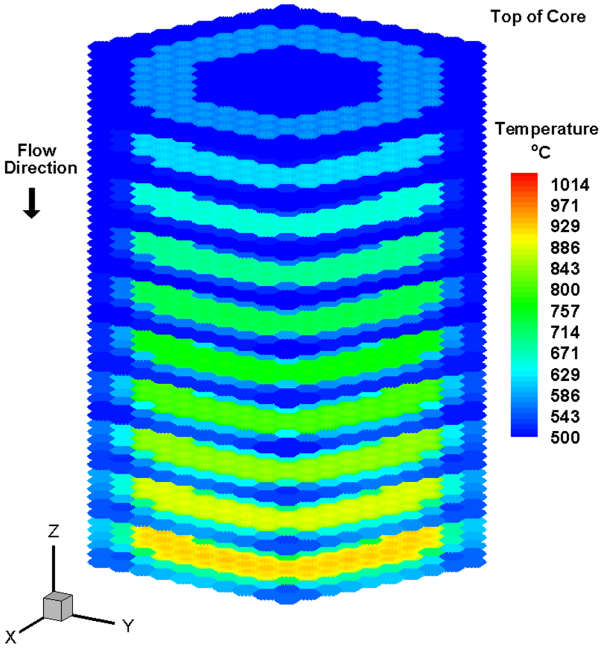

Figure 5.7 Graphite GT-MHR base-case, 3-D core temperature plot

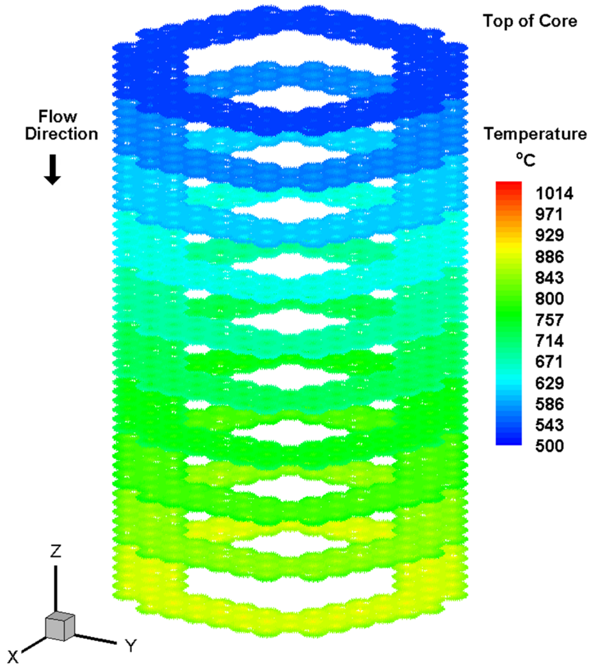

Figure 5.8 Coolant GT-MHR base-case, 3-D core temperature plot

Steady state temperature profiles for the GT-MHR show the same trends as in the MHTGR. A major concern for the GT-MHR, the MHTGR, and other design variations, is whether vessel steel and main loop components can withstand helium temperatures in excess of 850°C. Peak graphite and fuel temperatures are not a concern because they are well below the expected 1600°C thermal design limit. The peak and average GT-MHR core temperatures are shown in Table 5.2.

Table 5.2 GT-MHR base-case core temperatures

Material	Peak Temperature, [°C]	Average Temperature, [°C]
Fuel	1025.3	827.3
Graphite	933.5	574.9
Coolant	903.4	698.2

The average graphite temperature is only 85°C above the inlet coolant temperature. The MHTGR average graphite temperature is 117°C above the inlet coolant temperature. The GT-MHR model has nine assembly rings in the core. The MHTGR model only has seven assembly rings. The ratio of active fuel to total assembly blocks for the GT-MHR and MHTGR is 0.38 and 0.43 respectively. Having more reflector blocks increases bypass flow and reflector heat transfer area. This leads to a lower average graphite block temperature for similar heat fluxes between the core and reflector regions. A lower steady state average graphite block temperature is important for certain accident scenarios that rely on the high thermal storage capacity of the graphite blocks.

The coolant inlet temperature difference between the GT-MHR and the MHTGR is 231°C. The coolant design outlet temperature difference between the GT-MHR and the MHTGR is 160°C. The temperature rise for the MHTGR is 71°C greater than the GT-MHR. Table 5.3 shows the differences between the GT-MHR and MHTGR in peak and average temperature differences.

Table 5.3 Base-case core temperature differences between the GT-MHR and MHTGR

Material	Difference of Peak, °C	Difference of Average, °C
Fuel	163.7	187.8
Graphite	162.2	199.2
Coolant	163.3	194.6

The difference of core temperatures, compared to the difference of inlet and outlet coolant temperatures is important from a design efficiency standpoint. The difference of peak temperatures indicates that peak core temperatures are strongly related to the coolant outlet temperature. The difference of average core temperatures is roughly half of the difference between the inlet and outlet temperature differences. This shows a strong relation between average core temperature and the coolant temperature rise through the core.

The GT-MHR vessel arrangement and coolant flow path is identical to the MHTGR. The pressure drop for the GT-MHR base-case is 33.5 kPa. The GT-MHR has nearly twice the pressure drop compared to the MHTGR. This can be attributed to one main factor. The GT-MHR has twice the total core flow rate and a total flow area of only 1.55 times that of the MHTGR. Channel velocities are of the same factor higher for the GT-MHR. The frictional pressure drop for a representative large coolant channel in the MHTGR is 16 kPa/m. For the same coolant channel in the GT-MHR, the frictional pressure drop is 31 kPa/m. The GT-MHR, steady state mass flux distribution is plotted in Figure 5.9.

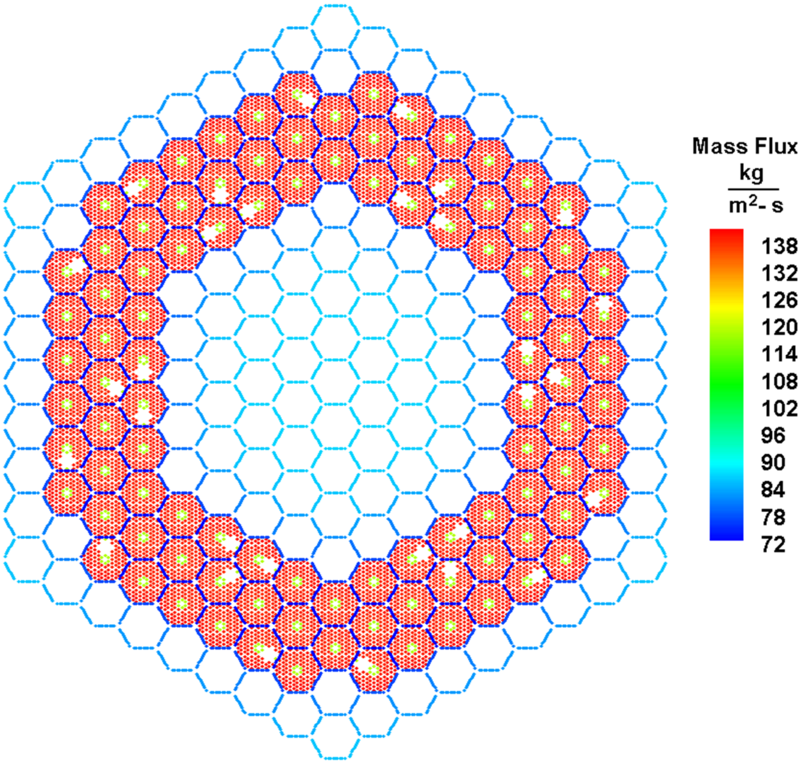

Figure 5.9 GT-MHR base-case mass flux distribution

The GT-MHR experiences a similar distribution as the MHTGR but with a higher average, absolute value. The difference between the highest and lowest mass flow value is nearly the same for both designs. Outside of the outer reflector block region is the permanent side reflector region. As discussed in the fluid modeling section, any gap spaces in that region are not modeled, including the possible side reflector-vessel wall gap space.

5.3 Design Parameter Variation

Parameters including bypass gap, axial power factor, and mass flow rate were varied to demonstrate the effect each parameter has on maximum and average core temperatures, and pressure drop. The differences from the steady state base case are also described and discussed in detail. Variations for both the MHTGR and the GT-MHR are discussed in this section and important differences between the two designs are highlighted.

5.3.1 Core Power Variation

The base-case is the uniform axial and radial power case described in the previous section. Three other cases were analyzed, which simulate different expected profiles through the life of the core. The first case assumes a “chopped” cosine power density shape, in which the peak occurs at the middle height of the core and the ends are at half of the core average power. The second case has the peak of the cosine curve in the bottom half of the core. This is judged to be a more realistic beginning-of-life profile due to the insertion of control rods from the top. The last case is a cosine curve with the peak toward the top of the core. This is judged to be a more realistic end-of-life core when the control rods are fully withdrawn. Different radial power distributions were not analyzed due to the complex nature of core neutronics for prismatic gas reactors.

Relative power is defined as the ratio of local power density to core average power density. The relative power profile shapes are dependent on the core axial discretization employed. All cases have the same total power (350 MW). For all the cases presented, the core height is discretized into ten uniform layers. Each layer is then physically represented as a single assembly block layer. Relative power for the four cases is shown in Figure 5.10. The step changes are shown to emphasize the axial discretization. Within each axial layer, a uniform power distribution is observed. Peak axial temperature profiles for the MHTGR and GT-MHR are shown in Figures 5.11 and 5.12 respectively. The power profile shape is also included to easily understand the

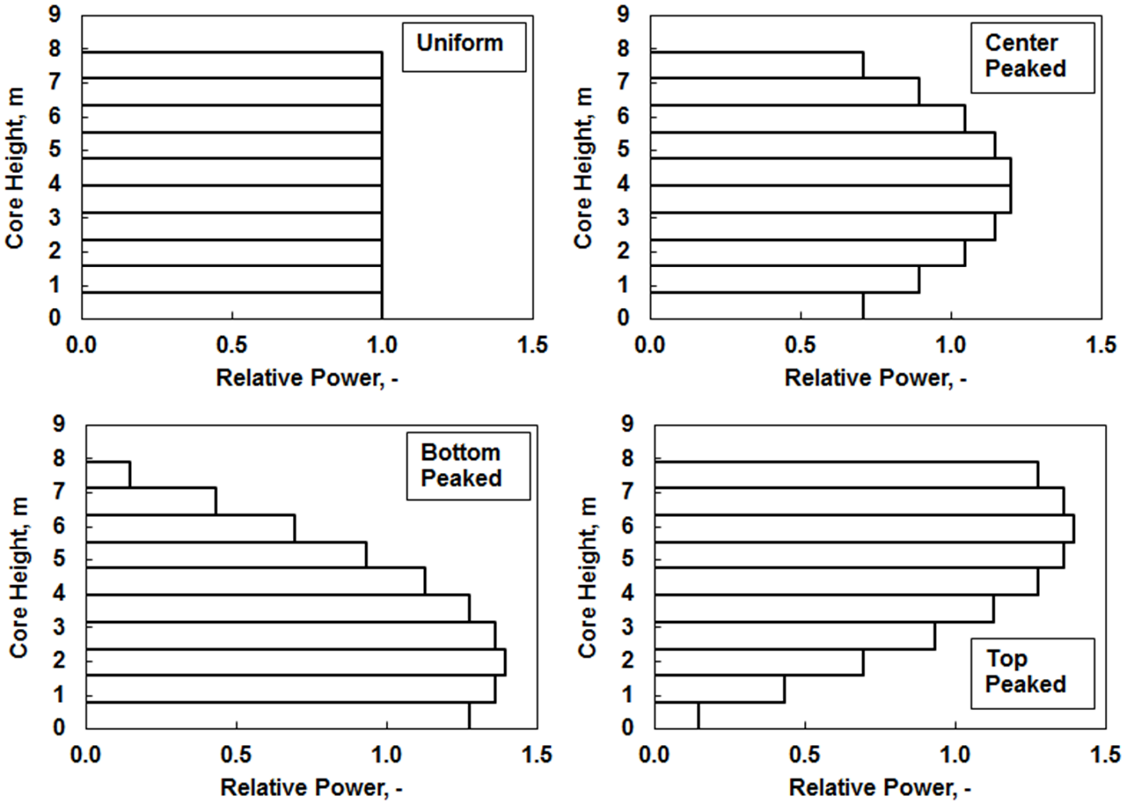

Figure 5.10 Axial relative power variations

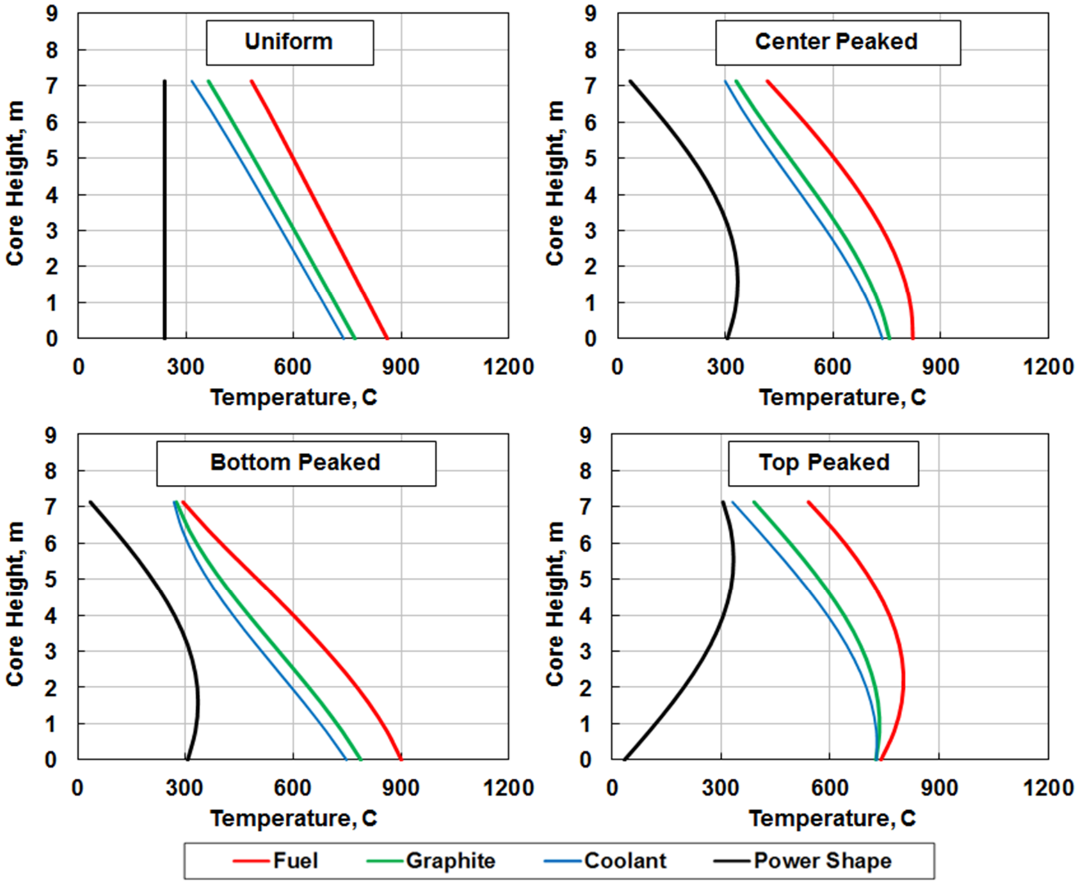

Figure 5.11 MHTGR peak axial temperature profiles

resulting temperature profiles.

Both designs exhibit similar trends for each axial power profile. The first observation is that heat conduction along the axial direction is minimal compared to the radial heat conduction. This is evident by the nearly uniform temperature difference between core materials for the uniform power case. This is expected, given the large axial length compared to the fuel pin-to-coolant channel radial distance.

Another important point to note, in the case of the top peaked core, is that fuel and graphite temperatures decrease toward the outlet. In all other cases, the fuel and graphite temperatures peak at the exit.

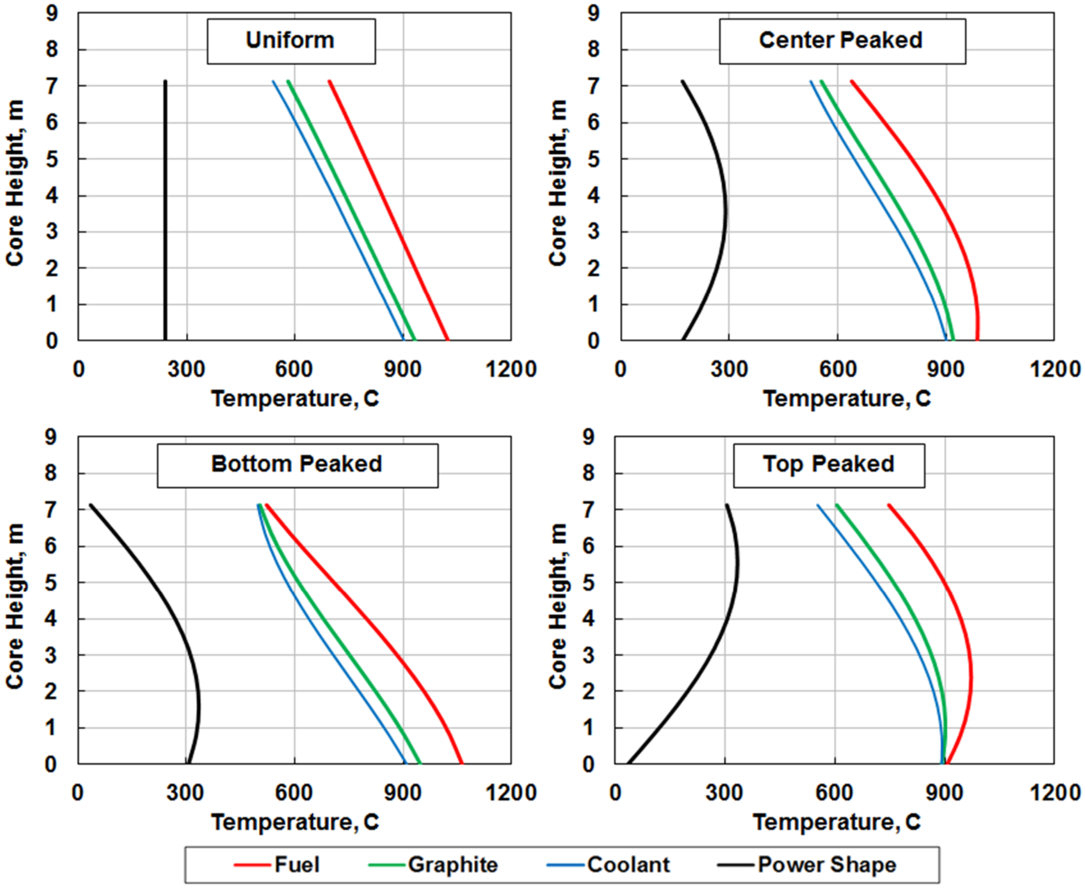

Figure 5.12 GT-MHR peak axial temperature profiles

The axial location of the peak may be important for safety design. If natural circulation is to play a major role in the redistribution of heat when forced circulation is immediately terminated, the location of the peak temperature effectively defines the fraction of the core that is heated by the naturally circulating fluid, and the fraction that heats up by graphite and fuel conduction only. The top peaked power profile would not be favorable then, because the lower 2.5 m would be near the coolant temperature, and thus would only be heated by axial conduction. For all other power shapes, the entire core length would be heated by the hot rising coolant. This would allow for a faster redistribution of core heat.

The bottom peaked axial power profile for both designs has the highest peak core temperatures. The top peaked axial power profile for both designs has the lowest peak core temperatures. The difference in peak fuel temperature between the top and bottom peaked case is about 100°C. Specifically for the MHTGR, all peak temperatures are well below expected TRISO design limits of around 1600°C. However, it is closer for the GT-MHR but still unlikely that peak temperatures could surpass 1600°C, for normal operation, considering the peak fuel temperature for the bottom axial power profile is only 1050°C.

The opposite is true for average core temperature. While the top peaked axial power profile has the highest peak fuel temperature, it has the lowest average fuel and graphite temperatures. In terms of reactor safety, this could be a better design choice because the difference in peak temperature is small (74°C for the fuel). Core average temperatures are important for the initial state of a transient sequence. For station backout, or loss of flow cases, the transient is expected to progress slowly, and the core sensible heat up time is expected to play a significant role in the transient outcome. Small differences in average core temperature can greatly affect the amount of sensible heating available in the core. The average core temperature for the bottom peaked case is 786°C for the fuel, and 556°C for the graphite. For the top peaked case the average core temperature is 867°C for the fuel, and 592°C for the graphite.

For normal operation thermal hydraulic design of LWRs, the peak fuel (or cladding) temperature is usually the basis for which additional design factors, such as measurement uncertainties, are applied to ensure that margins of safety are sufficient. For HTGRs, with slow transient heat up times, it may be better to choose the steady state average core temperature as the safety design parameter. In this case, a bottom peaked power distribution would yield the greatest margin of safety. If peak temperature is used, then a top peaked power distribution would yield the greatest margin of safety. For both cases, transient simulations would need to be performed, to verify that peak fuel temperature does not exceed the threshold value. The figure of merit for determining whether peak or the average temperature should be used would be the time to peak fuel temperature threshold crossing.

5.3.2 Bypass Gap Width Variation

Bypass gap width is an important parameter for both normal operation and safety design. Because core assembly blocks are designed to be replaced for refueling and maintenance, some gap is needed for operator movement. Manufacturing tolerances, radiation swell, and movement during refueling contribute to gap width uncertainty. Bypass gap width has been identified (Lee et al, 2006) as being important to core thermal hydraulic modeling accuracy, although at present with only a low to moderate understanding of its impact on core material temperatures.

Several different uniform bypass gap widths ranging from 1 mm to 4 mm for the MHTGR, and from 1 mm to 4.5 mm for the GT-MHR, were tested and the maximum fuel, graphite, and coolant temperatures were recorded. A uniform power profile was assumed and all other parameters, such as mass flow, were set to their reference values (see Table 1.1). Tables 5.4 and 5.5 contain key results of the bypass variation studies for the MHTGR and GT-MHR respectively.

Table 5.4 MHTGR bypass gap width variation results

Gap width [mm]	Peak fuel [°C]	Peak graphite [°C]	Peak coolant [°C]	Pressure drop [kPa]	Bypass flow [%]
4.0	877.4	788.1	764.7	15.7	15.5
3.5	867.8	778.0	761.1	16.6	12.7
3.1	861.6	771.3	758.8	17.3	10.6
2.5	853.5	762.7	756.2	18.4	7.4
2.0	848.1	757.0	754.6	19.2	5.0
1.5	843.9	752.6	752.6	19.9	3.0
1.0	841.0	749.5	749.5	20.5	1.5

Table 5.5 GT-MHR bypass gap width variation results

Gap width [mm]	Peak fuel [°C]	Peak graphite [°C]	Peak coolant [°C]	Pressure drop [kPa]	Bypass flow [%]
4.5	1047.9	957.3	923.2	28.5	19.4
4.0	1039.1	948.1	920.5	30.3	16.4
3.5	1031.0	939.5	918.7	32.1	13.5
3.1	1025.3	933.5	917.5	33.5	11.3
2.5	1016.9	924.7	916.0	35.7	7.95
2.0	1011.0	918.4	915.1	37.3	5.49
1.5	1006.0	913.2	913.2	38.9	3.36
1.0	1003.0	910.1	910.1	40.1	1.63

Both the MHTGR and GT-MHR show similar trends. The GT-MHR is on average 160°C cooler than the MHTGR. The pressure drop is twice is high for the GT-MHR and bypass flow is only slightly higher. For both designs, pressure drop decreases by 25% when the bypass gap is increased from 1 to 4 mm. Peak core temperatures listed in the above tables are illustrated in Figures 5.13 and 5.14 for the MHTGR and GT-MHR respectively.

Only a slight increase in peak fuel temperatures occurs when bypass gap size is increased from 1 to 4 mm. This is due to reduced graphite temperatures along the active fuel assembly boundary, which increases the graphite assembly heat flux from the center to the periphery. This slightly compensates for the reduced convective heat removal in the center of the assembly. For small gap sizes (< 2 mm), peak outlet coolant temperatures are observed in the low mass flux bypass channels in the active core region. As gap size decreases, the coolant approaches the wall surface (graphite) temperature quicker. For larger gap sizes (> 2 mm), peak outlet coolant temperatures are observed in the small, innermost coolant channels. This shift in where the peak occurs, either in bypass channels or small coolant channels, is due to the increase in total core flow area as bypass gap width is increased. From 1 mm to 4 mm, average fuel temperatures for the

MHTGR temperatures rise 15°C while graphite temperatures decrease by 128°C. The reduction in average graphite temperature is due to enhanced heat removal along the active fuel block assembly periphery. The peak temperatures all rise as bypass gap increases.

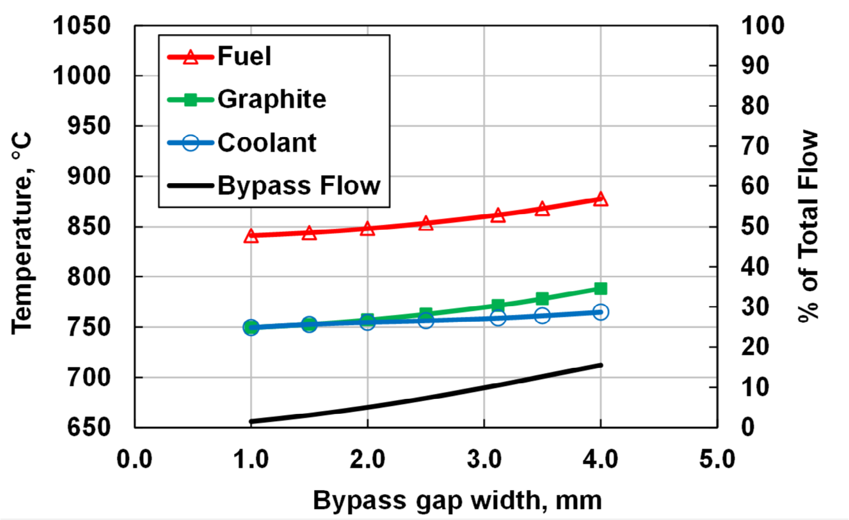

Figure 5.13 MHTGR peak core temperatures for various bypass gap sizes

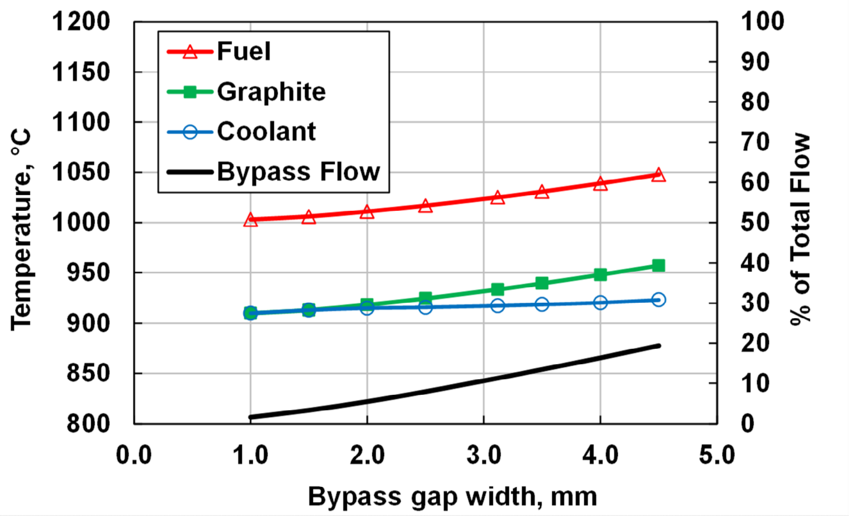

Figure 5.14 GT-MHR peak core temperatures for various bypass gap sizes

Because a major part of the core is composed of graphite, and the thermal storage capacity of fuel and graphite is similar, decreasing average graphite temperatures at the start of a transient could be more beneficial than slightly lowering peak fuel temperatures. Another benefit of the larger assembly bypass gaps is that pressure drop is reduced by 25%. The main advantage would be at shutdown, while natural circulation occurs. Lower flow resistance would increase natural circulation from the core, and to the vessel walls. Containment passive heat removal systems would be more efficient, providing a higher safety margin.

5.3.3 Mass Flow Rate Variation

The total core coolant flow rate is an important parameter for both normal operation and transient safety. The flow rate determines peak temperatures for a fixed inlet temperature. The flow rate can be tuned by plant operators to achieve a certain coolant exit temperature. For safety design, as the core heats up, the initial core temperature contributes to the amount of time available before a threshold is crossed, such as fuel failure or successful conduction cooldown. As the core heats up, decay power reduces, which reduces the natural convection and core heat conduction transient requirements. Lower initial peak and average temperatures are desirable from a safety point of view.

Total core coolant flow was varied between 90 and 110 % of the reference, expected flow rate. For the GT-MHR, the reference flow rate is 320 kg/s. For the MHTGR, the reference flow rate is 157.1 kg/s. Tables 6.6 and 6.7 contain key flow and temperature results for various mass flow rates.

Table 5.6 MHTGR mass flow rate variation results

Core flow rate [%]	Ave. coolant velocity [m/s]	Ave. Re [-]	Peak fuel [°C]	Peak graphite [°C]	Peak coolant [°C]	Ave. coolant [°C]	Pressure drop [kPa]
110 %	23.5	48,415	821.2	728.4	714.3	649.4	19.9
105 %	22.5	46,216	840.3	748.8	735.4	667.9	18.6
100 %	21.4	43,991	861.6	771.3	758.8	688.8	17.3
95 %	20.3	41,893	885.2	796.3	784.8	711.3	16.0
90 %	19.4	39,877	911.4	824.0	813.3	736.2	14.9

Table 5.7 GT-MHR mass flow rate variation results

Core flow rate [%]	Ave. coolant velocity [m/s]	Ave. Re [-]	Peak fuel [°C]	Peak graphite [°C]	Peak coolant [°C]	Ave. coolant [°C]	Pressure drop [kPa]
110 %	41.6	54,940	990.1	896.3	879.6	818.4	39.0
105 %	39.5	52,069	1006.9	914.0	897.7	834.1	36.2
100 %	37.6	49,556	1025.3	933.5	917.5	851.3	33.5
95 %	35.7	47,097	1046.7	956.0	940.1	871.5	32.5
90 %	33.8	44,528	1068.4	978.9	963.5	891.6	28.4

Bypass flow fraction did not change by increasing or decreasing total core flow. Bypass flow is 10.6% for the MHTGR, and 11.3% for the GT-MHR. This signifies that bypass flow is primarily a function of core geometry and not of the fluid or thermal conditions in the core.

Reynolds numbers for the lowest flow case are still well above the laminar-turbulent transition criterion which implies that turbulent correlations can be safely applied for any normal operation HTGR design. At transient or shutdown, natural circulation conditions, Reynolds numbers would have to be reevaluated along with due consideration of the different driving forces. Peak and average coolant exit temperatures are illustrated in Figures 5.15 and 5.16.

For both the MHTGR and GT-MHR, a 45°C temperature drop in peak fuel, graphite, or coolant can be expected for a 10% increase in core flow rate. Average fuel temperatures decrease by 20°C and average graphite temperatures by 10°C for a 10% increase in core flow rate. Pressure drop increases by 16%. Because mass flow and power are proportional, this indicates that a 10% core thermal power up-rate, a value common for many currently operating LWRs in the US, could be easily achieved without drastically raising core temperatures. Transient and accident scenario heat removal would still need to be reevaluated, with due consideration of the buoyancy, gravitational and frictional forces.

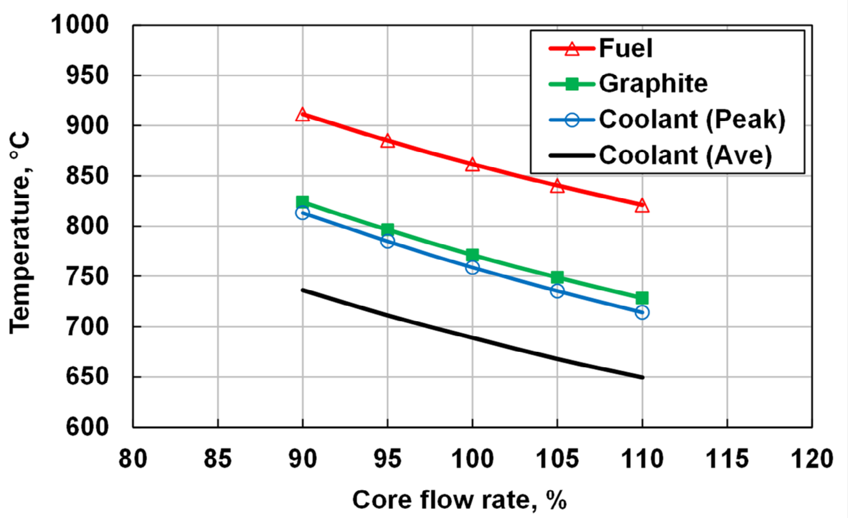

Figure 5.15 MHTGR peak core temperatures for various mass flow rates

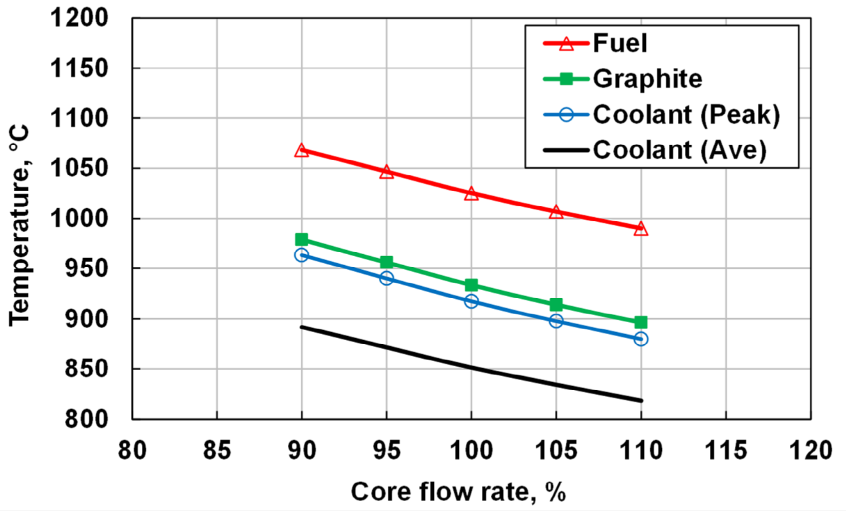

Figure 5.16 GT-MHR peak core temperatures for various mass flow rates

5.4 Comparison of Results with Similar Studies

The steady state results presented for the GT-MHR are compared to two CFD studies that examine the heat transfer within prismatic assembly blocks. In the study by Tak et al. (2008), the CFX 11 code was used with the standard k-ε turbulence model. In the study by Sato et al. (2010), the FLUENT code was used with both the standard k-ε turbulence model by Launder and Spalding, and the Wilcox k-ω turbulence model. Results from the standard k-ε turbulence analyses are compared here.

Both studies model a 1/12th sector of an active fuel assembly block. A grid of 2 million cells was applied in the study by Tak et al. (2008). A grid of 7.6 million cells was applied in the study by Sato et al. (2010). For the same geometry, a total of 980 unit cells are modeled in the present study. However, the whole core was still simulated and only the results for the comparison 1/12th model are presented.

A uniform power profile is assumed in both studies. There were slight differences in mass flow inlet conditions, and assembly power, which will be discussed in more detail in the following sections. The inlet pressure for both studies was 7 MPa.

5.4.1 Comparison with Tak et al. (2008)

In the study by Tak et al. (2008), several thermal fluid conditions differed from the GT-MHR parameters. A new steady state simulation (New case 1) was run with the revised conditions. Because the total core flow rate corresponding to the new 1/12th assembly flow rate was unknown, several steady state simulations were executed with decreasing total core flow, until the average desired coolant outlet temperature (950°C) was reached. The new conditions are compared against the GT-MHR values in Table 5.8.

Table 5.8 Comparison of thermal fluid design parameters with Tak et al. (2008)

Parameter	Tak et al. (2008)	GT-MHR	New case 1
Assembly power [MW]	5.88	6.07	5.88
1/12th assembly flow rate [kg/s]	0.205	0.260	0.202 (238)(1)
Average outlet temperature [°C]	950	850	950
Bypass gap width [mm]	1	3.12	1

(1) The corresponding total core flow rate is in the parentheses.

Graphite, fuel compact, and coolant temperatures are plotted in Figure 5.18 as a composite quantity, for a chosen axial plane, along the assembly radius shown in Figure 5.17. The maximum temperature plane for all cases occurs at the bottom of the core, near the coolant outlet.

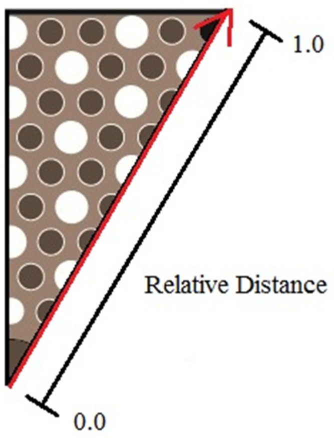

Figure 5.17 One-twelfth assembly model and radius line for temperature comparisons.

Two assemblies were chosen to compare with the reference 1/12th assembly model. Assembly 115 is the hottest assembly in the core, and lies in the central active fuel ring. Assembly 155 is a cooler active fuel assembly near the outer reflector ring. Composite temperature plots, along the assembly radius line, are shown in Figure 5.18.

The temperature peaks occur at fuel compact locations, while the temperature

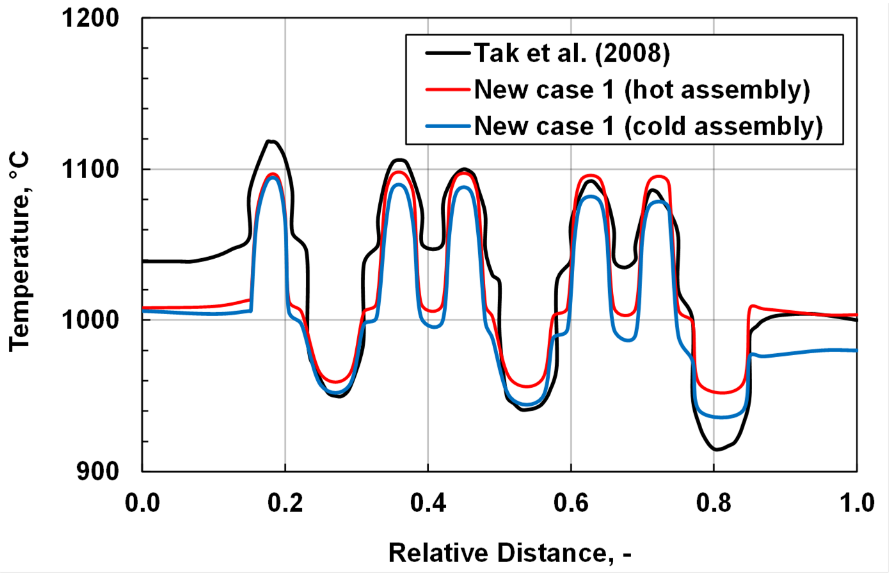

Figure 5.18 One-twelfth assembly, composite temperatures along the assembly radius line compared with Tak et. al (2008).

valleys occur at coolant channel locations. Between the fuel compacts and coolant channels is graphite.

In the hot assembly center, temperatures are 15°C lower than the reference case. With the exception of the coolant, temperatures near the hot assembly boundary are nearly equal. Only a 10°C temperature difference in the graphite is observed in the hot assembly, from the center to the assembly block boundary. A 21°C temperature difference is observed in the cold assembly, which is nearly equal to the reference analysis. The coolant temperature plotted, for both the hot and cold assembly, is the channel average temperature for the hottest axial plane. No attempt has been made to resolve the radial temperature profile for the coolant, as shown in the CFD analysis.

The pressure drop predicted in the reference analysis is 25.2 kPa. The pressure drop predicted here is 25.3 kPa. This pressure drop difference can be attributed to several factors. If the coolant velocities were equal, the pressure drop difference would be slightly higher. The coolant velocities in the hot assembly are 1.5% lower than in the reference analysis. However, the main factor for the difference is that wall shear stress, or frictional pressure drop, is approximated better by a fine grid than the coarse, 10 axial node, fluid model employed for this analysis. Other factors include fluid temperature differences, channel average velocity differences, and correlation uncertainty.

5.4.2 Comparison with Sato et al. (2010)

Thermal fluid conditions used in the study by Sato et al. (2010) are compared with values for the GT-MHR, and for the new simulation (New case 2), in Table 5.9. The desired outlet coolant temperature specified in the paper was 850°C. Upon inspection of the temperature results, however, the average outlet temperature for the given assembly flow rate was near 950°C. This is expected because the assembly flow rate was nearly equal to that used in the study by Tak et al. (2008). Similar to the last comparison, several simulations were performed until the average outlet temperature matched the comparison study.

The same assemblies chosen in the previous comparison are used here. A temperature plot for the 1/12th assembly model, with 3 mm bypass gap, predicted by Sato et al. (2010) is compared to the similar hot and cold assembly temperatures simulated in the “New case 2” run. Figures 5.19 and 5.20 show the hot and cold assembly comparisons, respectively.

Table 5.9 Comparison of thermal fluid design parameters to Sato et al. (2010)

Parameter	Sato et al. (2010)	GT-MHR	New case 2
Assembly power [MW]	6.07	6.07	6.07
1/12th assembly flow rate [kg/s]	0.200	0.260	0.210 (256)(1)
Average outlet temperature [°C]	950(2)	850	950
Bypass gap width [mm]	3.00	3.12	3.00

(1) The corresponding total core flow rate is in the parentheses.

(2) The average outlet temperature is mentioned to be 850°C, but results show that it is actually 950°C.

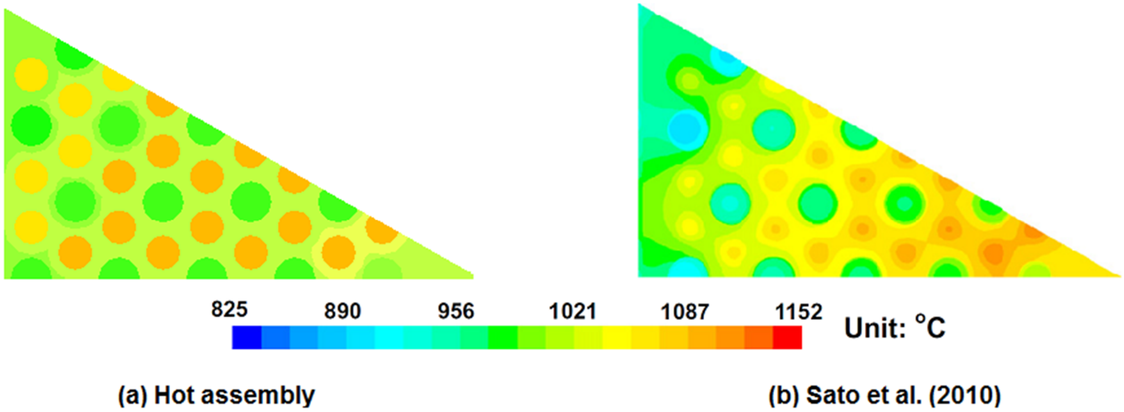

(a) Hot assembly

(b) Sato et al. (2010)

Figure 5.19 One-twelfth assembly, temperature profile from Sato et al. (2010) compared with assembly 115.

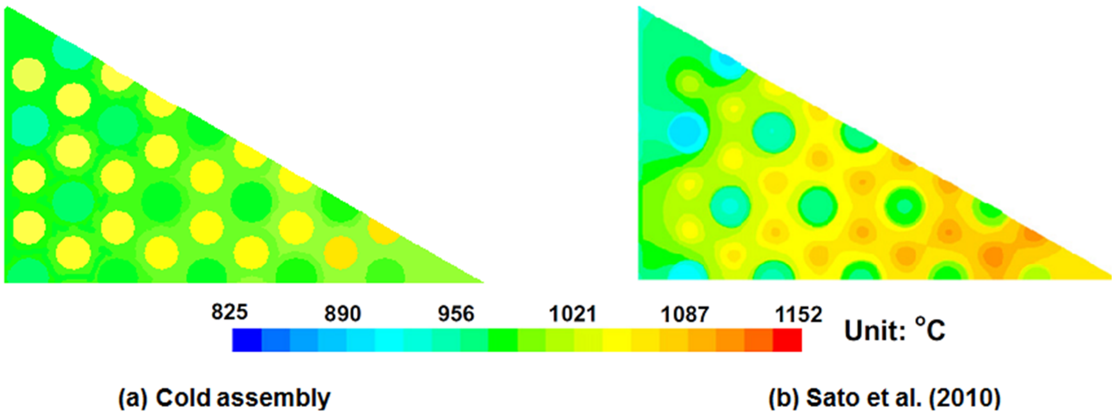

Figure 5.20 One-twelfth assembly, temperature profile from Sato et al. (2010) compared with assembly 155.

The temperature gradient from the assembly center to the assembly boundary is lower for both assemblies than what is predicted in the reference study. In the previous comparison, the temperature gradient in the cold assembly was near that of the reference study. One interesting feature that is more visible in the hot assembly is that peak graphite temperatures are predicted to be in the same region, just outside the assembly center point. The coldest region of graphite within each assembly is also predicted by both analyzes to be in the same region, near the assembly corners.

However, for both comparisons, the average graphite temperatures are lower than the values predicted by the CFD studies. One reason could be that the convective heat transfer coefficients are estimated to be larger than those estimated in the CFD studies. For the same power, higher convective heat transfer coefficients yields lower temperature differences between the graphite and coolant. The fuel-to-graphite thermal resistance may also be overestimated, compared to the CFD studies, because fuel temperatures are similar but the graphite temperatures are lower. This is observed in Figure 5.18, as the fuel pin peaks are larger than those predicted in the reference study.

The pressure drop predicted by Sato et al. (2010) is 32.0 kPa. The pressure drop predicted here is 23.7 kPa. This difference is larger than the difference predicted in the previous comparison. Some of the possible reasons for a difference, listed for the previous comparison, are also applicable for this comparison. Another reason for the difference is that the pressure drop reported by Tak et al. (2008) is for only the active fuel height. The pressure reported by Sato et al. (2010) also includes frictional losses through the (one meter in length) upper and lower reflector blocks. Upper and lower reflector block resistances are not modeled in the present analysis. The amount of bypass flow also affects the pressure drop, as demonstrated in Tables 5.4 and 5.5. The bypass flow fraction reported by Sato et al. was 4.15%. The bypass flow fraction estimated in this analysis for the total core is 7.7%. For only the 1/12th hot assembly portion of the core, the bypass fraction is predicted to be 8%. It is estimated to be higher here because additional bypass flow occurs in the inner and outer reflector block regions. Based on Table 5.5, a reduction from 8% to 4% bypass flow could increase the pressure drop by ~ 3 kPa. Both of these factors, neglecting the additional frictional losses in the upper and lower reflector blocks, and the increase in bypass flow, contribute to the lower pressure drop.

6. CONCLUSIONS

A method to analyze prismatic HTGRs using a coupled 1-D steady state axial flow model for whole core design and analysis was presented. The level of detail used within each assembly block is between CFD analysis like that of Cioni et al. (2006) and unit cell design codes like that of POKE by General Atomics, which is described in the report by Shenoy and McEachern (1974). The benefit of an intermediate scale code is that it allows for sufficient modeling and core detail while keeping the computational demand at an acceptable level. This allows for whole core design, optimization, parametric and sensitivity studies which otherwise would not be possible with detailed CFD models.

A benefit of the 1-D axial flow model is its ability to predict the channel mass flow distribution and bypass flow fraction. The mass flow distribution is found by enforcing uniform pressure conditions at the inlet and outlet, computing the pressure drops for several trial mass flow rates, and using a linear relationship to guess the new mass flow distribution that satisfies the pressure drop criteria. Bypass flow is also predicted by modeling six thin rectangular channels around each assembly block. The fluid 1-D energy, mass, and momentum equations are solved for the outlet properties using the inlet conditions and applicable friction factor and Nusselt number correlations. When steady state is reached, average channel outlet temperature is verified against its design value.

Core heat transfer is computed by discretizing each active fuel assembly block into graphite unit cells that contain either a fuel pin or coolant channel in a hexagonal lattice. Each fuel pin is further discretized in cylindrical geometry to capture the fuel temperature profile and heat transfer rate into the graphite. An explicit time discretization is used to converge on the steady state distribution using an arbitrary initial temperature distribution.

The method was then applied to two reactor designs: the GT-MHR, and the MHTGR. Both have a similar assembly design, but differ in total core power, power density, inlet/outlet temperature, mass flow rate, assembly block placement, and number of assembly blocks.

For a uniform power profile, steady state results for both designs have similar trends, but differ in inlet/outlet temperature. Axial temperature profile is linear while core radial temperatures are lower near the inner and outer reflectors. This is expected and implies that core power could also peak near the reflectors due to thermal feedback (along with enhanced local moderation). The average temperature difference between the two designs is around 200°C while the difference in peak temperatures is only around 163°C. Because the coolant velocity is lower for the MHTGR than for the GT-MHR, and both designs have comparable power density, the MHTGR has a slightly greater ΔT.

The choice of inlet temperature depends on the temperature limit of core components, range of acceptable core flow rates, and cycle design. For example, the MHTGR was originally designed to have a secondary Rankine power conversion cycle while the GT-MHR was designed to have a primary Brayton cycle. The rationale for the very high outlet temperatures does not apply for secondary steam cycle reactor designs, as the critical temperature for water is relatively low (374°C). High outlet temperatures are also desirable for process heat applications, but the reactor outlet temperature should be sufficiently higher than the application temperature. For the MHTGR, the outlet temperature is only 690°C.

In addition to the uniform power steady state cases, three parameter variation studies were performed to assess the impact of axial power profile, bypass gap, and mass flow rate on core temperature and mass flow distributions.

Bypass gap width is an important uncertainty and design parameter. Block movement, radiation induced dimensional changes, and assembly tolerances contribute to bypass gap uncertainty. Fuel and reactor vendors also have some control over the specifications of the gap width design. Depending on the steady state and transient safety analyses, a large or small bypass gap could be desired. The steady state analysis performed here indicates that a larger bypass gap would more desirable because average core temperatures are reduced by an order of magnitude more than the peak temperature increase. Larger bypass gaps also reduce the frictional pressure drop. However, peak coolant temperature increases, which may present a challenge to lower plenum structures if flow mixing is not adequate.

A change in mass flow rate has the effect of either lowering or raising core temperatures, for a constant power. The magnitude of core temperature change for a change in mass flow is important for reactor operators to know, particularly for operators of a coupled process heat plant and power conversion loop. The steam generator, primary heat exchanger, or other power conversion components may have strict inlet temperature requirements that may change if the process heat plant experiences a transient or goes offline. It may be necessary under some circumstances to change the core outlet temperature by altering the core flow rate.

Axial power profile is important to understand because over the life of the core, fuel depletion will shift the power peak as control rods or other reactivity control mechanisms change to maintain core criticality. The three axial power profiles included: a center-peaked cosine, top-peaked cosine, and a bottom-peaked cosine. The center-peaked cosine profile yielded average and peak temperatures similar to the uniform power case. The bottom-peaked power profile had the highest peak core temperatures, but also had the lowest average temperature. The top peaked power profile had the lowest peak core temperature, but had the highest average temperature. Both parameters need to be considered and are tabulated for each case discussed in this thesis.

Without analyzing the key accident scenarios, it is unclear if peak fuel temperature or average graphite temperature is the more favorable parameter for safety margin estimation of HTGRs. Steady state peak fuel temperature is often the key parameter for safety margin estimation of commercial LWRs because it can be related to the time to incipient melt, after the water boils away. A major difference between HTGRs and commercial LWRs is that the moderator (graphite) will increase in temperature without phase change during an accident. The time to fuel failure would thus be longer as the graphite would continually act as a source of heat removal as the fuel heats up.

For loss of forced circulation accidents, after control rods insert and core power begins to decrease, fuel temperatures will begin to rise. The rate of fuel temperature rise will decrease as decay heat decreases, and as the heat conduction rate from the fuel to the graphite increases. This will lead to a maximum or plateau in fuel temperature if the heat removal rate at the vessel/core boundary is equal to the heat generation rate. This is called a successful heat conduction cool down accident if the maximum temperature is less than the fuel failure temperature limit. If the limit is surpassed, then it is unsuccessful. It could be unsuccessful if the fuel starting temperature (steady state peak fuel temperature) is too high or if the core average graphite temperature is too high. The core average graphite temperature controls the heat conduction rate out of the fuel. A lower starting core average graphite temperature will slow the fuel temperature rise, allowing more time for decay heat to diminish to the value corresponding to the vessel heat removal rate at the fuel failure temperature limit. Transient safety analysis, with sufficient graphite heat conduction modeling in the core, is needed to establish whether steady state peak fuel temperature or average graphite temperature is the critical safety parameter.

It is important to note that the fuel failure limit, discussed in the preceding paragraphs, will be based on regulation set by the NRC and it will not necessarily guarantee that a TRISO fuel particle will fail at a specific temperature, but rather, it will represent a conservative estimate based on experimentally observed fuel failure mechanisms at various temperatures for TRISO type fuels.

While the computations preformed in this study provide several valuable insights, several aspects of the analysis could be improved. These areas include having a more refined graphite discretization, including bypass cross flow, including additional minor flow losses, improving the numerical performance, and benchmarking against another analysis or code. The graphite discretization could be enhanced by including cylindrical unit cells inside of the current hexagonal unit cell. The flow of heat within each unit cell could be better observed.

Modeling lateral bypass flow between blocks would be beneficial because lateral bypass flow would act to further reduce coolant channel flow, or increase the bypass flow fraction. The effect on average core temperature is unknown; however, peak temperatures would presumably rise. Including additional flow losses, such as entrance and exit flow area changes, would alter the mass flow distribution. Additional losses would act to flatten the mass flow distribution, or increase the bypass flow fraction. Based on the bypass gap width analysis, this would primarily be a benefit as average temperatures decreased substantially.

The numerical performance could be improved by implementing an implicit or semi-implicit Runge-Kutta method for time differencing. This would allow for larger time steps to be taken and possibly longer simulations to further ensure steady state convergence has been achieved. Trial and error determination of the time step size may not be necessary as is the case for explicit methods.

The method developed here could be greatly improved by performing a comprehensive benchmark comparison against another systems code such as RELAP, or fluid dynamics code such as Fluent. However, there are multiple challenges with this. The first challenge is verification of mass flow distribution. Because channel heat transfer is coupled to the fluid flow, simple 1-D pipe flow analysis tools would be insufficient for determining the flow distribution because the flow distribution affects the channel boundary conditions. A CFD analysis would need to model at least a 1/6th symmetric slice of the core for an accurate mass flow distribution. The reviewed papers that use CFD for HTGR steady state thermal hydraulic analyses have so far only included single assembly modeling. RELAP and system codes are often not capable of predicting individual channel flow rates, but rather lump neighboring channels (within an assembly for example) as having equivalent thermal and flow characteristics.

The second challenge is verification of the unit cell heat transfer models. This is an easier challenge because the same channel mass flow rates predicted by this method can be used, and the resulting core temperatures compared. The comparisons with the two studies, one by Tak et al. (2008), and another by Sato et al. (2008), are a good first approximation of verification. However, a more in-depth verification study would compare heat conduction rates, in the graphite and fuel compact, and convective heat transfer rates in the coolant channels, in addition to the resulting temperature profiles. The individual channel mass flow rates were also not aligned specifically to the values presented in the two studies. Rather, the total core flow rate was adjusted until the appropriate average coolant outlet temperature was reached. A separate CFD or other analysis would be necessary to obtain as much information as possible, to perform an as comprehensive as possible verification study.

Finally, the method developed here offers unique possibilities in two additional analysis areas. The first is coupling to a neutronics method using the pin-power input file, and temperature output files. Accurate pin powers provided by an external neutronics code could produce significantly more realistic temperature distributions than those presented in this thesis. Likewise, accurate temperatures computed by the presented method could enhance the neutronic calculations by resolving thermal feedback effects. The second possibility is the potential for select transient scenario simulations. The core heat conduction and energy balance calculations already rely on time-dependent terms for steady state computations. A time-dependent power profile, or pin-power input file, could easily be incorporated, and would simulate decay heat production. For loss-of-flow or loss-of-coolant accidents, significant additions to these analyses to account for natural circulation, and vessel and containment volumes would be required.

REFERENCES

Anderson, N., Hassan, Y. and Schultz, R. "Analysis of the Hot Gas Flow in the Outlet Plenum of the Very High Temperature Reactor Using Coupled Relap5-3D System Code and a CFD Code," *Nuclear Engineering and Design*, **238**, pp. 274-279 (2008).

Ball, S. J., "Next Generation Nuclear Plant Phenomena Identification and Ranking Tables (PIRTS)," *U.S. NRC*, NUREG/CR-6944, **2** (2008).

Bieder, U. and Graffard, E. "Qualification of the CFD Code Trio_U for Full Scale Reactor Applications," *Nuclear Engineering and Design*, **238**, pp. 671-679 (2008).

Bradshaw, G. B., Marsh, N. I. and Wallroth, C. F., "Safety Analysis Report for Fort St. Vrain Test Elements FTE-1 through FTE-8," *General Atomics*, GA-A13903 (1976).

Churchill, S. W. "Friction-Factor Equation Spans All Fluid-Flow Regimes," *Chemical Engineering* (New York), **84**, pp. 91-92 (1977).

Cioni, O., Marchand, M., Geffraye, G. and Ducros, F. "3D Thermal-Hydraulic Calculations of a Modular Block-Type HTR Core," *Nuclear Engineering and Design*, **236**, pp. 565- 573 (2006).

Damian, F., "VHTR Core Preliminary Analysis Using Nephtis3/Cast3m Coupled Modeling," 4th International Topical Meeting on High Temperature Reactor Technology, Washington DC, USA, September 28-October 1, 2008 (2008).

Demick, L., "Next Generation Nuclear Plant Pre-Conceptual Design Report," *Idaho National Laboratory*, INL/EXT-07-12967 (2007).

Futterer, M. A., Besson, D., Billot, P., Bogusch, E., Buckthorpe, D., Carluec, B., Casalta, S., Chauvet, V., Van Heek, A., Hittner, D., Von Lensa, W., Phelip, M., Pirson, J., Scheuermann, W. and Verrier, D., "RAPHAEL: The European Union's (Very) High Temperature Reactor Technology Project," American Nuclear Society Embedded Topical Meeting - 2006 International Congress on Advances in Nuclear Power Plants, ICAPP'06, June 4, 2006 - June 8, 2006, Reno, NV, United States (2006).

General Atomics, "Gas Turbine-Modular Helium Reactor (GT-MHR) Conceptual Design Description Report," 910720. (1996).

Gibbs, G. A., "Basis for NGNP Reactor Design Down-Selection," *Idaho National Laboratory*, INL/EXT-10-19565 (2010).

Johnson, R. W., "Development of a CFD Analysis Plan for the First VHTR Standard Problem," 2008 4th International Topical Meeting on High Temperature Reactor Technology, HTR 2008, September 28, 2008 - October 1, 2008, Washington, DC, United States (2008).

Johnson, R. W., Sato, H. and Schultz, R. R., "CFD Analysis of Core Bypass Phenomena," *Idaho National Laboratory*, INL/EXT-09-16882 (2009).

Lee, C. H., Zhong, Z., Taiwo, T. A., Yang, W. S., Smith, M. A. and Palmiotti, G., "Status of Reactor Physics Activities on Cross Section Generation and Functionalization for the Prismatic Very High Temperature Reactor, and Development of Spatially-Heterogeneous Codes," *Argonne National Laboratory*, ANL-GenIV-075 (2006).

Macdonald, P. E., "NGNP Preliminary Point Design – Results of the Initial Neutronics and Thermal-Hydraulic Assessments," *Idaho National Engineering and Environmental Laboratory*, INEEL/EXT-03-00870 Rev. 1 (2003).

McEligot, D. M. and McCreery, G. E., "Scaling Studies and Conceptual Experiment Designs for NGNP CFD Assessment," *Idaho National Engineering and Environmental Laboratory*, INEEL/EXT-04-02502 (2004).

McIlroy Jr, H. M., McEligot, D. M. and Pink, R. J. "Measurement of Turbulent Flow Phenomena for the Lower Plenum of a Prismatic Gas-Cooled Reactor," *Nuclear Engineering and Design*, **240**, pp. 416-428 (2010).

NGNP Industry Alliance, "NGNP Industry Alliance Announces Nuclear Technology Selection of AREVA Prismatic Block Modular Reactor Design," (2012).

Ryskamp, J. M., "Next Generation Nuclear Plant High-Level Functions and Requirements," *Idaho National Engineering and Environmental Laboratory*, INEEL/EXT-03-01163 (2003).

Sato, H., Johnson, R. and Schultz, R. "Computational Fluid Dynamic Analysis of Core Bypass Flow Phenomena in a Prismatic VHTR," *Annals of Nuclear Energy*, **37**, pp. 1172-1185 (2010).

Shenoy, A. S. and Mceachern, D. W., "HTGR Core Thermal Design Methods and Analysis," *General Atomics*, GA-A12985 (1974).

Tak, Nam.-Il., Kim, M.-H. and Lee, W. J. "Numerical Investigation of a Heat Transfer within the Prismatic Fuel Assembly of a Very High Temperature Reactor," *Annals of Nuclear Energy*, **35**, pp. 1892-1899 (2008).

Tsvetkov, P. V., Alanjo, A. B., Ames, D., Pritchard, M. L. “Spectrum shifting as a mechanism to improve performance of VHTRs with advanced actinide fuels,” *14th International Conference on Nuclear Engineering(ICONE14)*, Miami, Florida, July 17 – 20, 2006 (2006).

U.S. DOE, "A Technology Roadmap for Generation Iv Nuclear Energy Systems," GIF-002-00. (2002).

U.S. DOE, "Next Generation Nuclear Plant: A Report to Congress," (2010).

U.S. DOE, "Letter from Doe Secretary, Steven Chu, to the Chairman of the Subcommittee on Energy and Water Development, Dianne Feinstein," (October 17, 2011) (2011).

Williams, P. M., King, T. L. and Wilson, J. N., "Draft Preapplication Safety Evaluation Report for the Modular High-Temperature Gas-Cooled Reactor," *U.S. NRC*, NUREG-1338. (1989).

Zhi-Qing, W. "Study on Correction Coefficients of Laminar and Turbulent Entrance Region Effect in Round Pipe," *Applied Mathematics and Mechanics*, **3**, pp. 433-446 (1982).